Available online at www.sciencedirect.com
SCIENCE DIRECT®
Journal of Sound and Vibration 286 (2005) 477–506
JOURNAL OF SOUND AND VIBRATION
www.elsevier.com/locate/jsvi

Back-scattering correction and further extensions of Amiet's trailing-edge noise model. Part 1: theory

Michel Roger[a,*], Stéphane Moreau[b]

[a]*Ecole Centrale de Lyon, LMFA, UMR CNRS 5509, 69134 Ecully Cedex, France*
[b]*Valeo Motors and Actuators, 78321 La Verrière, France*

Received 9 October 2003; received in revised form 10 October 2004; accepted 11 October 2004
Available online 16 February 2005

Abstract

A previously published analytical formulation aimed at predicting broadband trailing-edge noise of subsonic airfoils is extended here to account for all the effects due to a limited chord length, and to infer the far-field radiation off the mid-span plane. Three-dimensional gusts are used to simulate the incident aerodynamic wall pressure that is scattered as acoustic waves. A leading-edge back-scattering correction is derived, based on the solution of an equivalent Schwarzschild problem, and added to the original formula. The full solution is found to agree very well with other analytical results based on a vanishing Mach number Green's function tailored to a finite-chord flat plate and sources close to the trailing edge. Furthermore, it is valid for any subsonic ambient mean flow velocity. The back-scattering correction is shown to have a significant effect at lower reduced frequencies, for which the airfoil chord is acoustically compact, and at the transition between supercritical and subcritical gusts. It may be important for small-size airfoils, such as automotive fan blades and similar technologies. The final far-field noise formula can be used to predict trailing-edge noise in an arbitrary configuration, provided that a minimum statistical description of the aerodynamic pressure fluctuations on the airfoil surface close to the trailing edge is available.

*Corresponding author. Tel.: +33 4 72 186011; fax: +33 4 72 189143.
E-mail address: michel.roger@ec-lyon.fr (M. Roger).

0022-460X/$ - see front matter © 2005 Elsevier Ltd. All rights reserved.
doi:10.1016/j.jsv.2004.10.054

Nomenclature

$c = 2b$	airfoil chord length
c_0	sound speed in quiescent medium
I	radiation integral
k	acoustic wavenumber
K	convective wavenumber
K_1, K_2	streamwise and spanwise aerodynamic wavenumbers
l_y	spanwise correlation length
L	airfoil span length
M	free-stream Mach number
p, p', P	fluctuating pressure variables
p_K	acoustic far-field pressure per wavenumber
R_s, R_t, S_0	corrected distances for convection effects
S_{pp}	far-field acoustic PSD
t	time
U	free-stream velocity
U_c	convection velocity
x_1, x_2, x_3	observer coordinate system
x, y, z	source coordinate system
X, Y, Z	source non-dimensional coordinate system
α	free-stream to convection speed ratio
β	compressibility parameter
γ^2	coherence function
ε	correction factor
κ, κ', μ	frequency parameters
Π_0	streamwise-integrated wavenumber spectral density of wall–pressure fluctuations
Π	wavenumber cross-spectral density of wall–pressure fluctuations
ϕ, Φ	disturbance potential
Φ_{pp}	wall pressure PSD
ψ, Ψ	modified acoustic potential
ρ_0	flow density in quiescent medium
ω	angular frequency

Superscripts

$\bar{(\cdot)}$	made non-dimensional by b

Subscripts

1	first-order scattering (trailing edge solution)
2	second-order back-scattering (leading edge solution)

1. Introduction

Broadband self-noise or trailing-edge noise, due to the scattering of blade boundary layer vortical disturbances into acoustic waves at the trailing edge, is a matter of primary interest, being the only remaining broadband noise contribution when a subsonic fan operates in a homogeneous stationary flow. It then defines the minimum achievable noise of a fan [1]. The concern for fan manufacturers is two-fold. Firstly, any installation effect generates more noise, making pure self-noise the lower limit to aim for when assessing low-noise designs. Secondly, self-noise can also be reduced if its origin and leading parameters are clearly identified, in terms of flow variables that can be varied through appropriate blade design. This latter point is especially crucial in wind turbine blade design for instance, since trailing-edge noise can be the major acoustic nuisance in that case [2–4].

Simple and easy-to-run prediction tools, that can be integrated in a fan design cycle, are currently needed. A minimum degree of physical realism is required but the details of the scattering process need not be reproduced exactly. Within the context of industrial applications, a physically consistent model has only to provide reliable A weighted levels or $\frac{1}{3}$ octave spectra at

any observer location. This means a realistic distribution of the radiated noise power with both frequency and angle of radiation, accurate enough for a definition in terms of decibels. Such tools can be provided using closed-form expressions deduced from analytical models. Semi-empirical methods have also been proposed [5–7]. Their limitation is that they can neither be extended to airfoil sections nor to radiation angles that are not in the database used to produce the method. The first analytical models were developed in the 1970s, with the initial work of Ffowcs Williams and Hall [8] being followed by Amiet's [9] and Howe's [10] theories, amongst others. All these formulations are based on the assumption of a semi-infinite airfoil, ignoring the leading edge. The argument is that the scattering process involves characteristic scales of the order of magnitude of the convected vortical eddies, much smaller than the chord length. More precisely, a half-plane Green's function is used in both [8,10]. In Amiet's work [9], the scattering equivalent sources are defined as if the airfoil were infinite in the upstream direction, but the radiation integral is calculated over the effective finite chord length. More recently, trailing-edge noise has received further attention [11]. It is recognized as a test case for numerical methods in Computational Aero-Acoustics (CAA) [12,13]. A time-domain formulation has also been proposed by Casper and Farassat [14]. A 2D computation of the Green's function tailored to a slightly cambered airfoil has also been performed by Oberai et al. [15].

Physically, blade self-noise results from the scattering of a boundary layer turbulent flow at the trailing edge. It can then be related either to the vortical, aerodynamic velocity field around the trailing edge or to the induced aerodynamic pressure field on the airfoil surface. The first approach, based on the velocity field, is outlined in Ref. [8] and was applied by Wang et al. [16] using Large Eddy Simulation (LES) results as input. Despite its great interest, it does not appear to be viable for industrial, fast turn-around applications. The same approach with a statistical description, thought as a post-processing of steady Reynolds–Averaged Navier Stokes (RANS) calculations, would be a less sophisticated way of addressing the question.

The second approach, based on the induced wall pressure, has been more thoroughly developed and applied, for instance by Brooks and Hodgson [17] and by Amiet [9,18]. However, it rarely addresses the connection with computational results. It is worth noting that now the vortical field is accounted for by means of its trace on the wall. This incident pressure is the equivalent acoustic source and is not to be confused with the full pressure, including the acoustic scattering. The question of whether or not the aerodynamic wall pressure can be used properly to determine the acoustic far-field pressure from experimental results may be still controversial. The point is taken for granted in this work, in view of the experimental evidence reported in the past in the case of a NACA-0012 symmetric airfoil [17]. It has been confirmed recently by Roger and Moreau [19], re-addressing the question of trailing-edge noise in the case of a thin cambered airfoil with rounded leading and trailing edges, by means of measurements made a couple of millimeters upstream of the trailing edge with flush-mounted pressure probes. At this location, the measured fluctuating level and convection speed showed that the wall pressure was essentially of aerodynamic nature. Indeed any aerodynamic pressure associated with a fully developed unsteady flow has a much higher level than the corresponding acoustic pressure, typically between 20 and 30 dB below.

The present work deals with an extension of Amiet's formulation and does consider the incident aerodynamic pressure as the origin of the sound. It is mainly concerned with analytical developments, aimed at predicting broadband self-noise from LES input data [20]. A back-scattering, leading-edge correction is first developed in Section 2 for incident 2D pressure gusts

using a two-step Schwarzschild's procedure [9,21]. This yields a modified chordwise distribution of the acoustic sources induced by the scattering mechanism. On the one hand, the full solution has the advantage of accounting for all the effects of a finite chord length. On the other hand, it has the same precision as the similar two-step solution also derived by Amiet to solve the complementary problem of the noise generated when upstream turbulence interacts with the leading edge of an airfoil [21]. The formulation is equivalent to the one derived by Howe [11] in the case of a vanishing Mach number. A 3D generalization is proposed in Section 3, with emphasis on oblique gusts and the subcritical regime, that appears not to have been investigated before. The far-field sound is addressed in Section 4, where the basic radiation integral is first derived for a single Fourier component of the incident pressure field. Then the power spectral density (PSD) of the acoustic pressure is related to the statistics of the aerodynamic wall pressure, including the radiation off the mid-span plane.

2. Generalized gust scattering formulae

2.1. Schwarzschild's solution

The following result, referred to as Schwarzschild's solution [22], is not demonstrated here. Let Φ be a 2D scalar field solution of the following wave problem:

$$\frac{\partial^2\Phi}{\partial x^2}+\frac{\partial^2\Phi}{\partial z^2}+\mu^2\Phi=0,$$
$$\Phi(x,0)=f(x),\quad x\geqslant 0,$$
$$\frac{\partial\Phi}{\partial z}(x,0)=0,\quad x<0.$$

Then for any $x<0$

$$\Phi(x,0)=\frac{1}{\pi}\int_0^\infty G(x,\xi,0)f(\xi)\,\mathrm{d}\xi$$

with

$$G(x,\xi,0)=\sqrt{\frac{-x}{\xi}}\,\frac{\mathrm{e}^{-\mathrm{i}\mu(\xi-x)}}{\xi-x}.$$

When addressing scattering problems in aeroacoustics, Amiet applies this result to determine the disturbance wall pressure generated when an incident vortical velocity field impinges on the leading edge of an airfoil [21] or when an incident (aerodynamic) wall pressure field is convected past the trailing edge [9]. The disturbance pressure then acts as equivalent acoustic sources and the far-field pressure is calculated by means of a radiation integral. In the second case, re-addressed here, the mathematical problem means that a full Kutta condition is assumed at the trailing edge. Note that this is again an unsolved question. Howe [10] pointed out that the unsteady Kutta condition might be only partially fulfilled, especially at higher frequencies. The application of Schwarzschild's procedure leads to mathematical solutions that are equivalent to the ones obtained by applying the Wiener–Hopf technique (see Ref. [23]).

2.2. Scattering of 2D pressure gusts

As a starting point for further developments, Amiet's original derivations are reproduced here for completeness. The airfoil is reduced to a flat plate with zero thickness and angle of attack, and with chord length $c = 2b$. The space is described by the streamwise coordinate x and the normal z coordinate, the fluid moving uniformly with velocity U. The trailing edge is at $x = 0$ (Fig. 1). Let us first consider that the incident aerodynamic wall pressure can be split into 2D Fourier components, defining pressure gusts with wave fronts parallel to the trailing edge. The convected wave equation in the plane normal to the airfoil is written as

$$\frac{\partial^2 p'}{\partial x^2} + \frac{\partial^2 p'}{\partial z^2} - \frac{1}{c_0^2}\left(\frac{\partial}{\partial t} + U\frac{\partial}{\partial x}\right)^2 p' = 0$$

with $p'(x, z, t) = P(x, z)\mathrm{e}^{\mathrm{i}\omega t}$ the disturbance pressure at reduced frequency ω. Thus, we obtain the complex equation

$$\beta^2 \frac{\partial^2 P}{\partial x^2} + \frac{\partial^2 P}{\partial z^2} - 2\mathrm{i}kM\frac{\partial P}{\partial x} + k^2 P = 0$$

with $k = \omega/c_0$ and $\beta^2 = 1 - M^2$, $M = U/c_0$ being the free stream Mach number, assumed lower than unity.

Performing the change of variable

$$P(x, z) = p(x, z)\mathrm{e}^{\mathrm{i}(kM/\beta^2)x}$$

yields

$$\beta^2 \frac{\partial^2 p}{\partial x^2} + \frac{\partial^2 p}{\partial z^2} + \left(\frac{KM}{\beta}\right)^2 p = 0$$

with $k = KM$ and $K = \omega/U$. By further transforming the problem with

$$X = \frac{x}{b}, \quad Z = \frac{\beta z}{b}, \quad \bar{K} = Kb, \quad \bar{\mu} = \frac{\bar{K}M}{\beta^2}$$

a canonical wave equation is obtained:

$$\frac{\partial^2 p}{\partial X^2} + \frac{\partial^2 p}{\partial Z^2} + \bar{\mu}^2 p = 0. \tag{1}$$

Fig. 1. Basic 2D problem with trailing-edge coordinates.

The airfoil extends over $-2 \leqslant X \leqslant 0$ in non-dimensional variables. Just upstream of the trailing edge, the incident gust is written as $p'(x,0,t) = \mathrm{e}^{\mathrm{i}\omega t}\mathrm{e}^{-\mathrm{i}\alpha Kx} = \mathrm{e}^{\mathrm{i}\omega t}\mathrm{e}^{-\mathrm{i}K_1 x} = P_0\mathrm{e}^{\mathrm{i}\omega t}$, with $\alpha = U/U_c$, U_c being the convection speed, lower than U.

In order to derive the main scattering term from Schwarzschild's solution, the airfoil is artificially extended to infinity upstream, covering $X<0$ [9]. P_0 must be cancelled in the wake according to the Kutta condition. This is done by adding a disturbance pressure P_1 such that $P = P_0 + P_1$ is zero for $X \geqslant 0$. Since the airfoil surface is assumed perfectly rigid, the normal derivative of P_1 must be zero for $X<0$. Finally, the following system of equations is obtained:

$$\begin{aligned} &\frac{\partial^2 p_1}{\partial X^2} + \frac{\partial^2 p_1}{\partial Z^2} + \bar{\mu}^2 p_1 = 0, \\ &\frac{\partial p_1}{\partial Z}(X,0) = 0, \quad X<0, \\ &p_1 = -\mathrm{e}^{-\mathrm{i}\bar{K}X[\alpha+(M^2/\beta^2)]}, \quad X \geqslant 0. \end{aligned} \tag{2}$$

Schwarzschild's solution then yields p_1 and thus P_1, for $X<0$ and $Z=0$

$$\begin{aligned} p_1(X,0) &= -\frac{1}{\pi}\int_0^\infty \sqrt{\frac{-X}{\xi}}\,\frac{\mathrm{e}^{-\mathrm{i}\bar{\mu}(\xi-X)}}{\xi - X}\,\mathrm{e}^{-\mathrm{i}\bar{K}\xi[\alpha+(M^2/\beta^2)]}\,\mathrm{d}\xi \\ &= -\frac{\mathrm{e}^{\mathrm{i}\bar{\mu}X}}{\pi}\int_0^\infty \sqrt{\frac{-X}{\xi}}\,\frac{\mathrm{e}^{-\mathrm{i}[\alpha\bar{K}+(1+M)\bar{\mu}]\xi}}{\xi - X}\,\mathrm{d}\xi. \end{aligned}$$

The preceding integral is calculated after straightforward manipulations (Ref. [24, p. 319])

$$\int_0^\infty \sqrt{\frac{-X}{\xi}}\,\frac{\mathrm{e}^{-\mathrm{i}A\xi}}{\xi - X}\,\mathrm{d}\xi = \pi\mathrm{e}^{-\mathrm{i}AX}\left[1 - \frac{\mathrm{e}^{\mathrm{i}\pi/4}}{\sqrt{\pi}}\int_0^{-AX}\frac{\mathrm{e}^{-\mathrm{i}t}}{\sqrt{t}}\,\mathrm{d}t\right]. \tag{3}$$

Let us introduce the complex function

$$E^*(x) = \int_0^x \frac{\mathrm{e}^{-\mathrm{i}t}}{\sqrt{2\pi t}}\,\mathrm{d}t = C_2(x) - \mathrm{i}S_2(x),$$

where C_2 and S_2 are Fresnel integrals (Ref. [26]). Then, since $\sqrt{2}\mathrm{e}^{\mathrm{i}\pi/4} = 1 + \mathrm{i}$, we get, for $X<0$

$$P_1(X,0) = \mathrm{e}^{-\mathrm{i}\alpha\bar{K}X}[(1+\mathrm{i})E^*(-[\alpha\bar{K} + (1+M)\bar{\mu}]X) - 1]. \tag{4}$$

This is the result derived by Amiet [9].

2.3. Leading edge back-scattering

Eq. (4) does not provide an exact solution, except for an infinite chord. It is only the main term, to be completed by a leading-edge correction. Indeed P_1 does not satisfy any specified condition on the potential in front of the airfoil leading edge, for $X < -2$. The needed correction is derived here, again using Schwarzschild's solution. First note that the disturbance pressure and potential are related by

$$P\mathrm{e}^{\mathrm{i}\omega t} = -\rho_0\,\frac{D\Phi}{Dt}$$

with $\Phi = \phi e^{i\omega t}$, ρ_0 being the undisturbed fluid density and D/Dt the substantial derivative. Equivalently, in reduced variables

$$-\frac{b}{\rho_0 U} P = \frac{\partial \phi}{\partial X} + i\bar{K}\phi \tag{5}$$

which leads to

$$\phi(X,0) = -\frac{b}{\rho_0 U} \int_{-\infty}^{X} P(\xi,0)\, e^{-i\bar{K}(X-\xi)}\, d\xi.$$

Thus the value of $P_1(X,0)$ provides that for the potential for $X<0$, as

$$\phi_1(X,0) = -\frac{b}{\rho_0 U} \int_{-\infty}^{X} e^{-i\alpha\bar{K}\xi}[(1+i)E^*(-\xi[\alpha\bar{K} + (1+M)\bar{\mu}]) - 1]\, e^{-i\bar{K}(X-\xi)}\, d\xi.$$

Integrating by parts and accounting for the property $E^*(\infty) = (1-i)/2 = 1/(1+i)$ yields

$$\phi_1(X,0) = \frac{b e^{-i\bar{K}X}}{i\rho_0 U(\alpha-1)\bar{K}} \{e^{-i(\alpha-1)\bar{K}X}\ [(1+i)E^*(-A_1 X) - 1] - \Theta[(1+i)E^*(-AX) - 1]\} \tag{6}$$

with

$$\Theta = \sqrt{\frac{A_1}{A}}, \quad A_1 = \bar{K_1} + (1+M)\bar{\mu}, \quad A = \bar{K} + (1+M)\bar{\mu}.$$

This potential must be now cancelled for $X < -2$ by adding a secondary potential correction, corresponding to the back-scattering. Strictly speaking, the condition to be applied is a zero potential at infinity [25]. Amiet's solution based on the Schwarzschild's technique imposes a zero potential for $X < -2$ instead. This is compatible with dipoles distributed normal to the flow. The same assumption is made here. A preliminary change of variable is needed in order to get another canonical Schwarzschild problem

$$\phi_1 = \psi_1 e^{i\bar{\mu}MX}, \quad v = -(X+2)$$

through which we introduce the ψ_2 potential such that $\psi_2(v,0) = -\psi_1(v,0)$ for $v>0$, i.e. $X < -2$, and

$$\frac{\partial \psi_2}{\partial Z}(v,0) = 0$$

for $v<0$, i.e. the surface of the airfoil plus an infinite extension downstream.

Now ψ_2 is a solution of the wave equation with parameter $\bar{\mu}$. Consequently, for $v<0$

$$\psi_2(v,0) = \frac{-1}{\pi} \int_0^{\infty} \sqrt{\frac{-v}{\xi}}\, \frac{e^{-i\bar{\mu}(\xi-v)}}{\xi - v} \psi_1(\xi,0)\, d\xi.$$

For convenience, the E^* function above can be related to the complementary complex error function [26]

$$(1+\mathrm{i})E^*(x)-1=-\mathrm{erfc}^*\left((1-\mathrm{i})\sqrt{\frac{x}{2}}\right)=-\mathrm{erfc}\left((1+\mathrm{i})\sqrt{\frac{x}{2}}\right)=-[1-\Phi^\circ(\sqrt{\mathrm{i}x})]$$

with the equivalent definitions

$$\Phi^\circ(Z)=\frac{1}{\sqrt{\pi}}\int_0^{Z^2}\frac{\mathrm{e}^{-z}}{\sqrt{z}}\,\mathrm{d}z \quad \text{and} \quad \Phi^\circ(\sqrt{\mathrm{i}x})=\sqrt{2}\mathrm{e}^{\mathrm{i}\pi/4}E^*(x)$$

so that Eq. (6) reads

$$\phi_1(X,0)=\frac{-b\mathrm{e}^{-\mathrm{i}\bar{K}X}}{\mathrm{i}\rho_0 U(\alpha-1)\bar{K}}\{\mathrm{e}^{-\mathrm{i}(\alpha-1)\bar{K}X}\,[1-\Phi^\circ(\sqrt{-\mathrm{i}A_1X})] - \Theta[1-\Phi^\circ(\sqrt{-\mathrm{i}AX})]\}. \tag{7}$$

Going to the total disturbance potential, we find

$$\phi_2(X,0)=\frac{b\sqrt{X+2}\,\mathrm{e}^{-\mathrm{i}\bar{\mu}(1-M)X}}{\mathrm{i}\pi\rho_0 U(\alpha-1)\bar{K}}[W_1(X+2)-\Theta W(X+2)] \tag{8}$$

with

$$W_1(X+2)=\int_0^\infty\frac{\mathrm{e}^{\mathrm{i}[\alpha\bar{K}+(M-1)\bar{\mu}](\xi+2)}}{(\xi+2+X)\sqrt{\xi}}\,\mathrm{erfc}\left(\frac{1+\mathrm{i}}{\sqrt{2}}\sqrt{A_1(\xi+2)}\right)\mathrm{d}\xi$$

and

$$W(X+2)=\int_0^\infty\frac{\mathrm{e}^{\mathrm{i}[\bar{K}+(M-1)\bar{\mu}](\xi+2)}}{(\xi+2+X)\sqrt{\xi}}\,\mathrm{erfc}\left(\frac{1+\mathrm{i}}{\sqrt{2}}\sqrt{A(\xi+2)}\right)\mathrm{d}\xi.$$

Since the derivations are made to get a correction, a consistent approximation is sufficient. Using classical expansions of the complementary error function [26] leads to

$$\sqrt{\pi}(1+\mathrm{i})x\,\mathrm{e}^{2\mathrm{i}x^2}\,\mathrm{erfc}[(1+\mathrm{i})x]=1+\sum_{m=1}^{\infty}\mathrm{i}^m\frac{1\cdot3\cdots(2m-1)}{(4x^2)^m}.$$

Practically, the argument remains large enough to allow for an expansion to the zeroth order. Thus

$$W_1(X+2)\simeq\frac{\sqrt{2}\,\mathrm{e}^{-\mathrm{i}4\bar{\mu}}}{(1+\mathrm{i})\sqrt{\pi}\sqrt{A_1}}\int_0^\infty\frac{\mathrm{e}^{-2\mathrm{i}\bar{\mu}\xi}}{\sqrt{\xi}\sqrt{\xi+2}(\xi+X+2)}\,\mathrm{d}\xi$$

and, by a further change of variable,

$$\phi_2(X,0)\simeq\frac{-b(1+\mathrm{i})\,\mathrm{e}^{-\mathrm{i}4\bar{\mu}}\,\mathrm{e}^{\mathrm{i}(M-1)\bar{\mu}X}}{\pi^{3/2}\rho_0 U(\alpha-1)\bar{K}\sqrt{2}\sqrt{A_1}}(1-\Theta^2)\mathscr{I}$$

is obtained with

$$\mathscr{I}=\int_0^\infty\frac{\mathrm{e}^{-2\mathrm{i}\bar{\mu}(X+2)x}}{\sqrt{x}\sqrt{2+(X+2)x}(1+x)}\,\mathrm{d}x$$

$\mathscr{I}$ has no analytic closed-form solution. A numerical evaluation would lead to additional derivatives when later deriving the wall pressure and the subsequent radiation integral. Again an approximation, consistent with numerical tests, is better. Indeed, $\xi + 2$ is larger than 2 and $\alpha\bar{K}$ is easily several units in the applications. This suggests the introduction of the following simplified integral, that is solvable analytically [24]:

$$\mathscr{I}' = \frac{1}{\sqrt{2}} \int_0^\infty \frac{\mathrm{e}^{-2\mathrm{i}\bar{\mu}(X+2)x}}{\sqrt{x}(1+x)} \mathrm{d}x = \frac{\pi}{\sqrt{2}} \mathrm{e}^{2\mathrm{i}\bar{\mu}(X+2)} [1 - (1+\mathrm{i})E^*(2\bar{\mu}(X+2))].$$

Comparison with the numerical computation of the exact integral shows that the preceding simplified integral need only be corrected on the imaginary part, provided that $\bar{\mu}$ does not approach zero, according to

$$\mathrm{Re}(\mathscr{I}) \simeq \mathrm{Re}(\mathscr{I}'), \quad \mathrm{Im}(\mathscr{I}) \simeq \varepsilon\, \mathrm{Im}(\mathscr{I}') \quad \text{with } \varepsilon = \left(1 + \frac{1}{4\bar{\mu}}\right)^{-1/2}.$$

The exact value of the integral and the approximate closed form solution are plotted in Fig. 2 for $\bar{\mu} = 1$, as an example. Numerical tests have proved the approximation to be satisfactory for acoustic calculations even at reasonably low frequencies (typically $\bar{\mu} = 0.05$). Discrepancies remain on the imaginary part. They will be overcome by the regularization procedure proposed in Section 4. Finally, Eq. (8) becomes

$$\phi_2(X,0) \simeq \left(\frac{-b}{\rho_0 U}\right) \frac{(1+\mathrm{i})\mathrm{e}^{-4\mathrm{i}\bar{\mu}}}{2\sqrt{\pi}(\alpha-1)\bar{K}} \frac{1-\Theta^2}{\sqrt{A_1}} \mathrm{e}^{\mathrm{i}(M-1)\bar{\mu}X} \times \{\mathrm{e}^{2\mathrm{i}\bar{\mu}(X+2)}[1 - (1+\mathrm{i})E^*(2\bar{\mu}(X+2))]\}^c, \tag{9}$$

the notation $\{.\}^c$ standing for an imaginary part multiplied by the correcting factor ε.

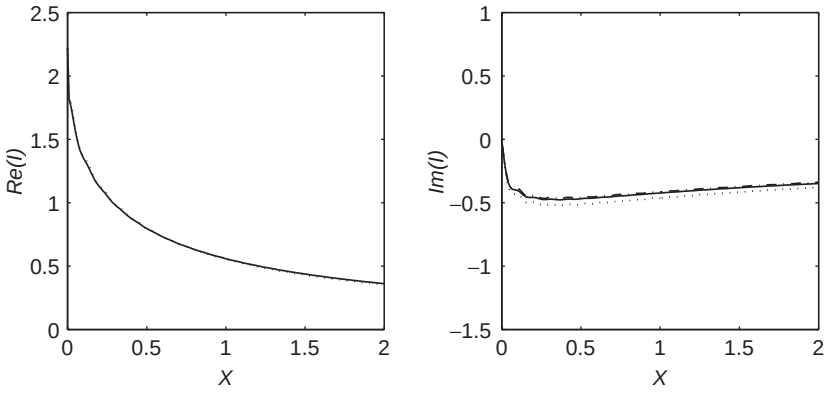

Fig. 2. Exact integral $\mathscr{I}$ and approximation. $M = 0.05$, $\bar{\mu} = 1$. —, numerical computation; - - -, simplified integral; -.-, approximation.

The last step is to deduce the back-scattering disturbance pressure from Eq. (5). Formally we have

$$P_2(X,0) \simeq \frac{(1+\mathrm{i})\mathrm{e}^{-4\mathrm{i}\bar{\mu}}}{2\sqrt{\pi}(\alpha-1)\bar{K}} \frac{1-\Theta^2}{\sqrt{A_1}} \mathrm{e}^{\mathrm{i}(M-1)\bar{\mu}X} \times \left\{ \mathrm{i}[\bar{K}+(M-1)\bar{\mu}]\{-\}^c + \left(\frac{\partial}{\partial X}\{-\}\right)^c \right\} \tag{10}$$

with the property that the correction of the imaginary part and the derivative with respect to X commute.

This back-scattering correction has been developed here because the induced loads do concentrate at the leading edge, in the same way as found in classical linearized theories of unsteady aerodynamics [21] (the derivative leading to P_2 generates a factor of $(X+2)^{-1/2}$). As a consequence, some quantitative evaluation is needed before concluding as to whether it can be neglected or not. Now P_2 does not satisfy the Kutta condition and should also be corrected in principle. Rigorous use of Schwarzschild's solution would lead to an iterative procedure with successive trailing- and leading-edge steps. The aforementioned application to the noise generation by upstream turbulence impinging on an airfoil [21] shows that the first two are enough. The same is assumed to hold here. More attention will be paid to this point in Section 4.1.

3. 3D gust solution

3.1. Wave equation

The most general incident wall pressure field convected past the trailing edge can be split by Fourier analysis into 2D wavenumbers with components K_1 and K_2 in the streamwise and spanwise directions, respectively. At a given frequency, each wavenumber corresponds to an oblique gust, leading to a 3D scattering problem. The Schwarzschild's solution must be recast, including the spanwise component, associated with the y coordinate. Since the trailing edge is assimilated to the edge of a half-plane extending to infinity along the spanwise y-axis, the generalization is straightforward. The spanwise dependence can be factorized, leading to a corrected form of the 2D problem of the preceding section.

The equation for the disturbance pressure now is written as

$$\frac{\partial^2 p'}{\partial x^2} + \frac{\partial^2 p'}{\partial z^2} + \frac{\partial^2 p'}{\partial y^2} - \frac{1}{c_0^2}\left(\frac{\partial}{\partial t} + U\frac{\partial}{\partial x}\right)^2 p' = 0.$$

The solution is sought in the form of

$$p'(x,y,z,t) = P(x,y,z)\mathrm{e}^{\mathrm{i}\omega t},$$
$$P(x,y,z) = p(x,z)\mathrm{e}^{\mathrm{i}(kM/\beta^2)x}\,\mathrm{e}^{-\mathrm{i}K_2 y}$$

compatible with the boundary conditions, and the incident wall pressure gust is generalized as

$$P_0 = \mathrm{e}^{-\mathrm{i}\alpha\bar{K}X}\,\mathrm{e}^{-\mathrm{i}\bar{K}_2 Y}$$

with $Y = y/b$. The wave equation becomes

$$\frac{\partial^2 p}{\partial X^2} + \frac{\partial^2 p}{\partial Z^2} + \bar{\kappa}^2 p = 0 \tag{11}$$

in which

$$\bar{\kappa}^2 = \bar{\mu}^2 - \frac{\bar{K}_2^2}{\beta^2}$$

and the canonical problem is recovered with $\bar{\kappa}$ instead of $\bar{\mu}$, provided that $\bar{\kappa}^2$ is positive. This implies that

$$|\bar{K}_2| < \frac{\bar{K}M}{\beta} = \frac{\bar{K}_1 M}{\alpha\beta}$$

with $\bar{K}_1 = \alpha\bar{K}$ the streamwise non-dimensional wavenumber.

All the derivations of Section 2 are easily extended in the 3D case, bearing in mind that $\bar{\mu}$ is replaced by $\bar{\kappa}$ in the wave equation but not in the change of variable between p and P. Eqs. (4), (9) and (10), respectively, become

$$P_1(X,0) = \mathrm{e}^{-\mathrm{i}\alpha\bar{K}X}[(1+\mathrm{i})E^*(-[\alpha\bar{K} + \bar{\kappa} + M\bar{\mu}]X) - 1],$$

$$\phi_2(X,0) \simeq \left(\frac{-b}{\rho_0 U}\right) \frac{(1+\mathrm{i})\mathrm{e}^{-4\mathrm{i}\bar{\kappa}}}{2\sqrt{\pi}(\alpha-1)\bar{K}} \frac{1-\Theta^2}{\sqrt{\alpha\bar{K} + M\bar{\mu} + \bar{\kappa}}} \mathrm{e}^{\mathrm{i}(M\bar{\mu}-\bar{\kappa})X} \times\{\mathrm{e}^{2\mathrm{i}\bar{\kappa}(X+2)}[1-(1+\mathrm{i})E^*(2\bar{\kappa}(X+2))]\}^c,$$

$$P_2(X,0) \simeq \frac{(1+\mathrm{i})\mathrm{e}^{-4\mathrm{i}\bar{\kappa}}}{2\sqrt{\pi}(\alpha-1)\bar{K}} \frac{1-\Theta^2}{\sqrt{\alpha\bar{K} + M\bar{\mu} + \bar{\kappa}}} \mathrm{e}^{\mathrm{i}(M\bar{\mu}-\bar{\kappa})X} \times\left\{\mathrm{i}[\bar{K} + M\bar{\mu} - \bar{\kappa}]\{-\}^c + \left(\frac{\partial}{\partial X}\{-\}\right)^c\right\},$$

$$\Theta = \sqrt{\frac{\bar{K}_1 + \bar{\mu}M + \bar{\kappa}}{\bar{K} + \bar{\mu}M + \bar{\kappa}}}.$$

Some numerical errors may occur when applying the analytical solution to a 3D gust, however, since $\bar{\kappa}$ is now allowed to approach zero for finite $\bar{\mu}$. This point will be emphasized later on in Section 4.1.

The present 3D analysis assumes that what happens at the span ends can be neglected, the induced disturbance wall pressure establishing itself as if the span was infinite. It holds rigorously if the spanwise extent of the trailing edge is large when compared to the aerodynamic wavelengths $2\pi/K_2$ that carry a significant energy in the incident turbulent pressure field, or the corresponding spanwise correlation lengths.

3.2. Subcritical gusts

If the preceding condition on $\bar{K}_2$ is not satisfied, an elliptic equation is obtained. Were the solution for the sound field directly sought from that equation in the whole space, the corresponding so-called subcritical pressure gusts would not radiate, essentially as a result of the assumption of infinite span. More precisely, they are expected to induce a field decaying exponentially from the airfoil surface, which means that the only contributors to the far field are the so-called supercritical gusts ($\bar{\kappa}^2 > 0$). In the present application, the field induced on the airfoil surface by all gusts including the subcritical ones is used as an acoustic source distribution. In the following section, the acoustic field will be obtained from this field by integrating over the actual airfoil surface. The subcritical gusts $\bar{\kappa}^2 < 0$ will then contribute to the radiated sound field due to the finite span. This is the reason why the behavior of the subcritical gusts is analyzed in this section. The special case $\bar{\kappa} = 0$ will be referred to as the cut-off condition. Note that the same splitting between elliptic and hyperbolic solutions arises in classical linearized theories of unsteady aerodynamics, as stated by Graham [25] and Amiet [21]. At a given Mach number, the main contribution to the radiation comes from the supercritical gusts, and thus the small spanwise wavenumbers. With increasing Mach number, more and more oblique gusts contribute significantly.

The subcritical solution can be inferred considering again Eq. (2) with a negative $\bar{\kappa}^2$ instead of $\bar{\mu}^2$. The square root must be chosen in order to ensure the expected decay. Using the relationship between E^* and Φ° yields the modified result

$$P_1(X,0) = -\mathrm{e}^{-\mathrm{i}\alpha\bar{K}X}[1 - \Phi^\circ([-\mathrm{i}(\alpha\bar{K} + M\mu - \mathrm{i}\bar{\kappa}')X]^{1/2})]$$

defining now

$$\bar{\kappa}' = \sqrt{\left(\frac{\bar{K}_2}{\beta}\right)^2 - \bar{\mu}^2}.$$

Sample numerical results are plotted in Fig. 3 for fixed values of the frequency and a low Mach number, with a progressive variation of $\bar{K}_2$ from 0 to $2\bar{\mu}$ corresponding to gusts passing from the supercritical to the subcritical range. A continuous transition is observed between both regimes. $\bar{K}_2$ is found to have a negligible effect on the supercritical solution P_1 (all dashed-lines curves almost collapse here for the small value of M), whereas increasing $\bar{K}_2$ in the subcritical case rapidly leads to a much faster decay upstream from the trailing edge, especially at higher frequencies. This is the illustration of the aforementioned filtering or cut-off.

A leading-edge back-scattering correction is to be developed also for subcritical gusts, even in view of the faster decay of P_1. Indeed, for 3D gusts close to the cut-off condition $\bar{\kappa}' = 0$, the equivalent Schwarzschild's solution involves a vanishingly small equivalent frequency in the reduced 2D problem, whatever the actual frequency might be.

$\phi_1(X,0)$ is again given by Eq. (7) in which A_1 and A are replaced by $A_1' = \bar{K}_1 + M\bar{\mu} - \mathrm{i}\bar{\kappa}'$ and $A' = \bar{K} + M\bar{\mu} - \mathrm{i}\bar{\kappa}'$, respectively and Θ by $\Theta' = \sqrt{A_1'/A'}$. The corresponding derivations are

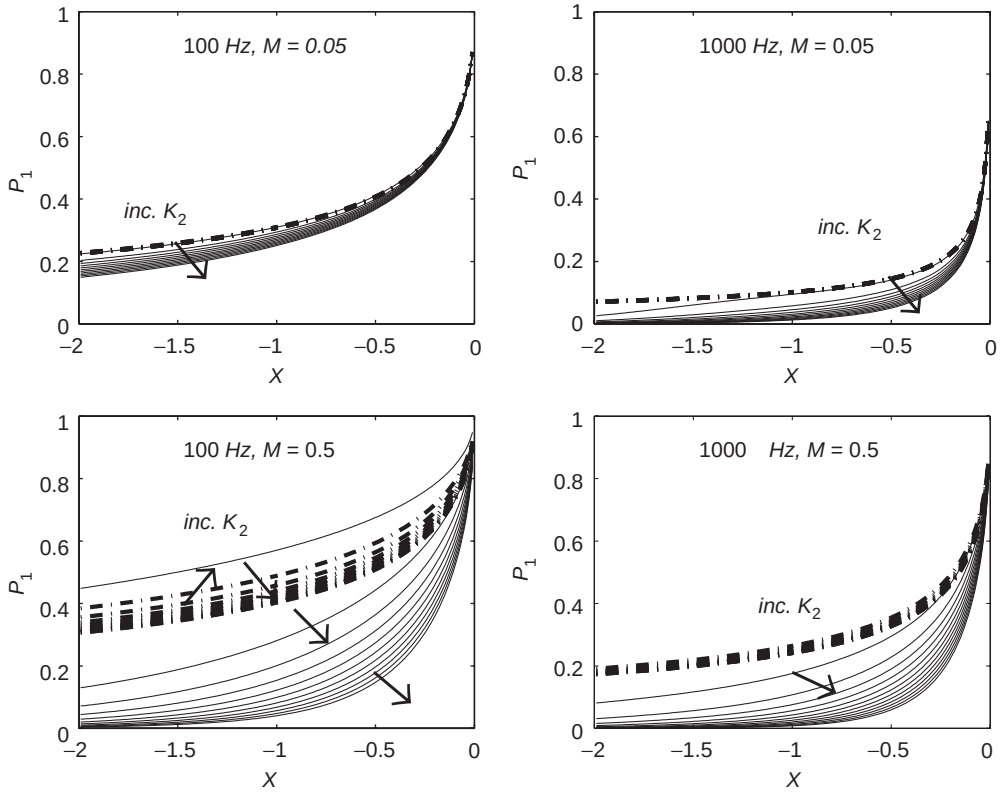

Fig. 3. Scattered pressure amplitude $|P_1|$ for supercritical (-.-) and subcritical (—) gusts. (left) $\bar{K} = 2$, $\bar{\mu} = 0.12$; (right) $\bar{K} = 20$, $\bar{\mu} = 1.2$. The variations with increasing $\bar{K}_2$ from 0 to $2\bar{\mu}$ by steps of $\bar{\mu}/10$ are indicated by arrows.

again similar to the ones in Section 2, leading to a modified Schwarzschild problem. Instead of the integral $\mathscr{I}$, a real integral is now found, that can be approximated without any correction according to

$$\mathscr{I} = \int_0^\infty \frac{\mathrm{e}^{-2\bar{\kappa}(X+2)x}}{\sqrt{x}(1+x)\sqrt{2+(X+2)\,x}}\,\mathrm{d}x \simeq \frac{1}{\sqrt{2}}\int_0^\infty \frac{\mathrm{e}^{-2\bar{\kappa}(X+2)x}}{\sqrt{x}(1+x)}\,\mathrm{d}x$$
$$= \frac{\pi}{\sqrt{2}}\,\mathrm{e}^{2\bar{\kappa}(X+2)}[1-\mathrm{erf}(\sqrt{2\,\bar{\kappa}(X+2)})]$$

and with the same restrictions of non-vanishing $\bar{\kappa}'$. The new expression for the back-scattering potential is

$$\phi_2(X,0) = \left(\frac{-b}{\rho_0 U}\right)\frac{(1+\mathrm{i})\,\mathrm{e}^{\mathrm{i}(M\bar{\mu}-\mathrm{i}\bar{\kappa})X}}{2\sqrt{\pi}(\alpha-1)\bar{K}\sqrt{A_1'}}(1-\Theta'^2)[1-\mathrm{erf}(\sqrt{2\bar{\kappa}(X+2)})]$$

from which P_2 is again easily obtained thanks to Eq. (5).

4. Far-field noise calculations

4.1. Radiation integral

The acoustic far-field pressure corresponding to a disturbance wall pressure of wavenumber $\mathbf{K} = (K_1, K_2)$ is given by the radiation integral, equivalently found in [21]

$$p_K(\mathbf{x},\omega) = \frac{-\mathrm{i}\omega x_3}{4\pi c_0 S_0^2} \int_{-2b}^{0} \int_{-L/2}^{L/2} \Delta P \, \mathrm{e}^{\mathrm{i}\omega R_t/c_0} \, \mathrm{d}y \, \mathrm{d}x,$$

where $\mathbf{x} = (x_1, x_2, x_3)$ stands for the observer location with the origin at the trailing edge center point (Fig. 4). Here $\Delta P = 2(P_1 + P_2) = 2P$ is the induced source distribution as given by the Schwarzschild's solution of Sections 2 and 3, function of the coordinates (x, y) on the airfoil. The factor 2 accounts for the opposite disturbance pressures induced on both sides of the airfoil when the incident pressure is scattered by the trailing edge, acting as equivalent lift fluctuations. The airfoil extends from $-L/2$ to $L/2$ in the spanwise direction.

The convection of the acoustic waves by the uniform external flow is accounted for through the modified coordinates

$$R_t = \frac{1}{\beta^2}\,(R_s - M(x_1 - x)),$$

$$R_s = S_0\left(1 - \frac{x_1 x + \beta^2 x_2 y}{S_0^2}\right),$$

$$S_0^2 = x_1^2 + \beta^2(x_2^2 + x_3^2).$$

P can be written as $P = f(X)\mathrm{e}^{-\mathrm{i}(\bar{K}_1 X + \bar{K}_2 Y)}$ as a function of the coordinates made non-dimensional by the half-chord length, f being the complex amplitude of the source distribution, according to the expressions of Sections 2 and 3. Then the radiation integral becomes

$$p_K(\mathbf{x},\omega) = \frac{-\mathrm{i}\omega x_3}{2\pi c_0 S_0^2}\, b^2 \int_{-2}^{0} \int_{-L/(2b)}^{L/(2b)} f(X)\mathrm{e}^{-\mathrm{i}(\bar{K}_1 X + \bar{K}_2 Y)} \times \mathrm{e}^{-\mathrm{i}\frac{k}{\beta^2}\left[S_0 - \frac{x_1 X + \beta^2 x_2 Y}{S_0} b - M(x_1 - bX)\right]} \mathrm{d}Y \, \mathrm{d}X.$$

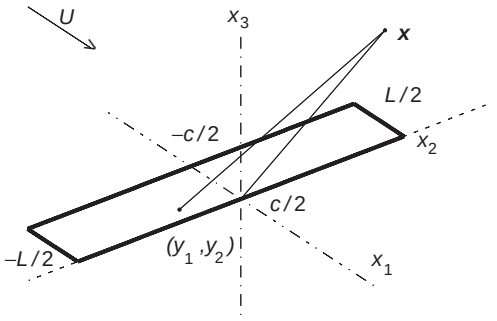

Fig. 4. Source and observer coordinates.

The integral involving Y is straightforward

$$b\int_{-L/(2b)}^{L/(2b)} \mathrm{e}^{-\mathrm{i}[\bar{K}_2-\bar{k}x_2/S_0]Y}\,\mathrm{d}Y = L\,\mathrm{sinc}\left\{\frac{L}{2b}\left(\bar{K}_2-\bar{k}\,\frac{x_2}{S_0}\right)\right\},$$

where $\mathrm{sinc}(x)$ stands for $\sin(x)/x$ and yields

$$p_K(\mathbf{x},\omega) = \frac{-\mathrm{i}\omega x_3 Lb}{2\pi c_0 S_0^2}\,\mathrm{sinc}\left\{\frac{L}{2b}\left(\bar{K}_2-\bar{k}\,\frac{x_2}{S_0}\right)\right\} \times \mathrm{e}^{-\mathrm{i}(k/\beta^2)(S_0-Mx_1)}\int_{-2}^{0} f(X)\mathrm{e}^{-\mathrm{i}CX}\,\mathrm{d}X \tag{12}$$

with

$$C = \bar{K}_1 - \bar{\mu}\left(\frac{x_1}{S_0}-M\right).$$

The analytical solution is derived first for the supercritical gust solution. For the main contribution P_1,

$$f_1(X) = (1+\mathrm{i})E^*(-BX) - 1,$$

$$B = \bar{K}_1 + M\,\bar{\mu} + \bar{\kappa}, \quad \bar{\kappa}^2 = \bar{\mu}^2 - \frac{\bar{K}_2^2}{\beta^2}.$$

Then integrating by parts we obtain

$$\int_{-2}^{0} f_1(X)\,\mathrm{e}^{-\mathrm{i}CX}\,\mathrm{d}X = \frac{1}{\mathrm{i}C}\,[1-\mathrm{e}^{2\mathrm{i}C}] + \frac{1+\mathrm{i}}{\mathrm{i}C}\,E^*(2B)\mathrm{e}^{2\mathrm{i}C} - \frac{1+\mathrm{i}}{\mathrm{i}C}\int_{-2}^{0}\frac{B\mathrm{e}^{-\mathrm{i}(C-B)X}}{\sqrt{-2\pi BX}}\,\mathrm{d}X$$

or

$$\int_{-2}^{0} f_1(X)\mathrm{e}^{-\mathrm{i}CX}\,\mathrm{d}X = -\frac{\mathrm{e}^{2\mathrm{i}C}}{\mathrm{i}C}\left\{(1+\mathrm{i})\mathrm{e}^{-2\mathrm{i}C}\sqrt{\frac{B}{B-C}}E^*[2(B-C)] - (1+\mathrm{i})E^*[2B] + 1 - \mathrm{e}^{-2\mathrm{i}C}\right\}. \tag{13}$$

This result is identical to Amiet's [9] in the special case $\bar{K}_2 = 0$. According to Amiet [18], the term $\mathrm{e}^{-2\mathrm{i}C}$ at the end of the curly brackets can be considered to balance the contribution of the incident field P_0 to the sound radiation. It must be discarded. The solution must also tend to the cardioid pattern, characteristic of the half-plane solution, as frequency goes to infinity.

The correction P_2 is then derived from

$$f_2(X) = H\,\mathrm{e}^{\mathrm{i}[\bar{K}_1+M\bar{\mu}-\bar{\kappa}]X}\left\{\mathrm{i}[\bar{K}+M\bar{\mu}-\bar{\kappa}]\{-\}^c + \left(\frac{\partial}{\partial X}\,\{-\}\right)^c\right\}$$

with

$$H = \frac{(1+\mathrm{i})\mathrm{e}^{-4\mathrm{i}\bar{\kappa}}\,(1-\Theta^2)}{2\sqrt{\pi}(\alpha-1)\bar{K}\sqrt{B}}$$

the curly bracket being defined in Section 2. The following integral needs to be calculated:

$$\mathscr{J} = \int_{-2}^{0} \mathrm{e}^{-\mathrm{i}D(X+2)}\{\mathrm{e}^{2\mathrm{i}\bar{\kappa}(X+2)}[1-(1+\mathrm{i})\,E^*(2\bar{\kappa}(X+2))]\}^c\,\mathrm{d}X$$

with $D = \bar{\kappa} - \bar{\mu}x_1/S_0$. The real and imaginary parts must be treated separately and some tedious algebra leads to

$$\mathscr{J} = -\frac{1+\varepsilon}{2}(1+\mathrm{i})\int_0^2 \mathrm{e}^{-\mathrm{i}(D-2\bar{\kappa})x}E^*(2\bar{\kappa}x)\,\mathrm{d}x - \frac{1-\varepsilon}{2}(1-\mathrm{i})\int_0^2 \mathrm{e}^{-\mathrm{i}(D+2\bar{\kappa})x}E(2\bar{\kappa}x)\,\mathrm{d}x.$$

Each remaining integral is again calculated by integrating by parts

$$\frac{1}{H}\int_{-2}^{0} f_2(X)\,\mathrm{e}^{-\mathrm{i}CX}\,\mathrm{d}X = \{\mathrm{e}^{4\mathrm{i}\bar{\kappa}}[1-(1+\mathrm{i})E^*(4\bar{\kappa})]\}^c - \mathrm{e}^{2\mathrm{i}D} + \mathrm{i}[D+\bar{K}+M\bar{\mu}-\bar{\kappa}]G \tag{14}$$

with

$$G = (1+\varepsilon)\,\mathrm{e}^{\mathrm{i}(2\bar{\kappa}+D)}\frac{\sin(D-2\bar{\kappa})}{D-2\bar{\kappa}} + (1-\varepsilon)\,\mathrm{e}^{\mathrm{i}(-2\bar{\kappa}+D)}\frac{\sin(D+2\bar{\kappa})}{D+2\bar{\kappa}} + \frac{(1+\varepsilon)(1-\mathrm{i})}{2(D-2\bar{\kappa})}\,\mathrm{e}^{4\mathrm{i}\bar{\kappa}}E^*(4\bar{\kappa}) - \frac{(1-\varepsilon)(1+\mathrm{i})}{2(D+2\bar{\kappa})}\,\mathrm{e}^{-4\mathrm{i}\bar{\kappa}}E(4\bar{\kappa}) + \frac{\mathrm{e}^{2\mathrm{i}D}}{2}\sqrt{\frac{2\bar{\kappa}}{D}}E^*(2D)\left[\frac{(1+\mathrm{i})(1-\varepsilon)}{D+2\bar{\kappa}} - \frac{(1-\mathrm{i})(1+\varepsilon)}{D-2\bar{\kappa}}\right].$$

The full expression of the acoustic pressure is then obtained from Eqs. (12)–(14). The main factor relating the far-field sound to the aerodynamic wall pressure field is the following radiation integral summing both contributions:

$$I(\bar{K}_1,\bar{K}_2) = \int_{-2}^{0} f(X)\,\mathrm{e}^{-\mathrm{i}CX}\,\mathrm{d}X \quad \text{with } f = f_1 + f_2.$$

The associated directivity pattern in terms of the product $|kcI|$ times x_3/S_0 is plotted in Fig. 5 for $\bar{K}_2 = 0$ (mid-span plane) at different low reduced frequencies and a very low Mach number ($M = 0.05$). The latter restriction emphasizes the main features of the radiation integral due to the limited chord length with no additional convection effects. It is also justified by the intended applications to low-speed fans. The solutions, however, are valid for any subsonic Mach number. The external flow direction is from left to right, parallel to the chord line, corresponding to the horizontal axis at angle 0°. The full calculation is plotted along with only the main trailing-edge scattering, and the leading-edge back-scattering is inferred from the difference. Note that the diagrams are symmetrical with respect to the axis since the theoretical trailing-edge noise radiation is in opposite phase on each side of the airfoil plane. This is well reproduced for instance by the computations of Singer et al. [13]. The expected two lobes characteristic of a compact dipole are obtained. The back-scattering correction is found partially to cancel the main

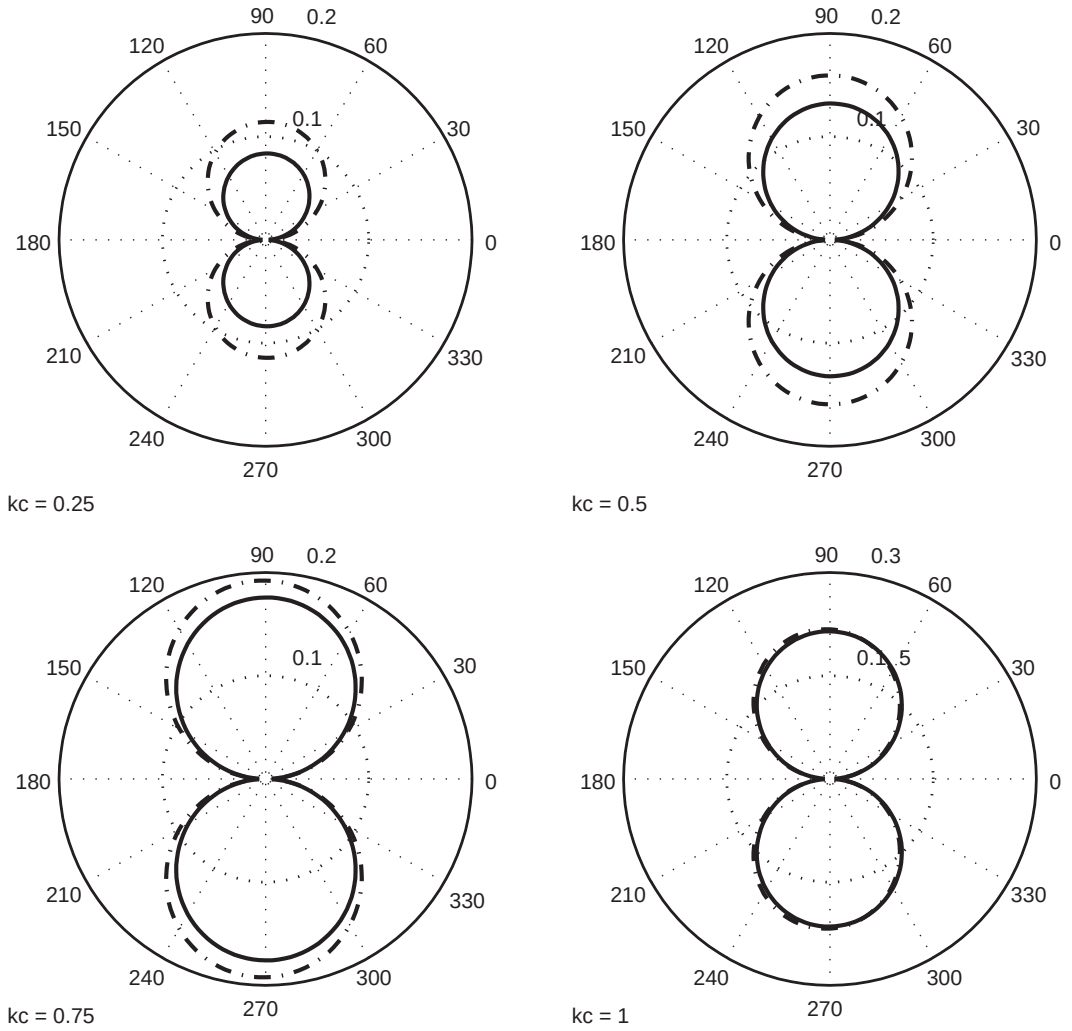

Fig. 5. Typical directivity patterns at low frequencies. $M = 0.05$. —, full solution: -.-, main term only.

trailing-edge contribution at lower frequencies. A systematic overestimate would then result from using the main term only. However, Eq. (14) may not be valid for arbitrarily small kc. At about $kc = 1$, the net effect of the correction becomes negligible.

Equivalent calculations are reported in Fig. 6 for higher frequencies. As frequency increases, the main lobes bend toward the leading edge and secondary lobes appear. The directivity diagram roughly tends to the asymptotic cardioid pattern associated with the edge scattering of a half-plane [8,10]. As expected, the leading-edge correction vanishes as the frequency increases. The resulting high-frequency behavior is equivalent to that which would be derived by just using the original Amiet's formulation. Furthermore, the directivity results of Fig. 6 are in very good agreement with Howe's results obtained at the same four reduced frequencies [11]. The latter work addresses the same mathematical problem, based on the vanishing Mach number Green's

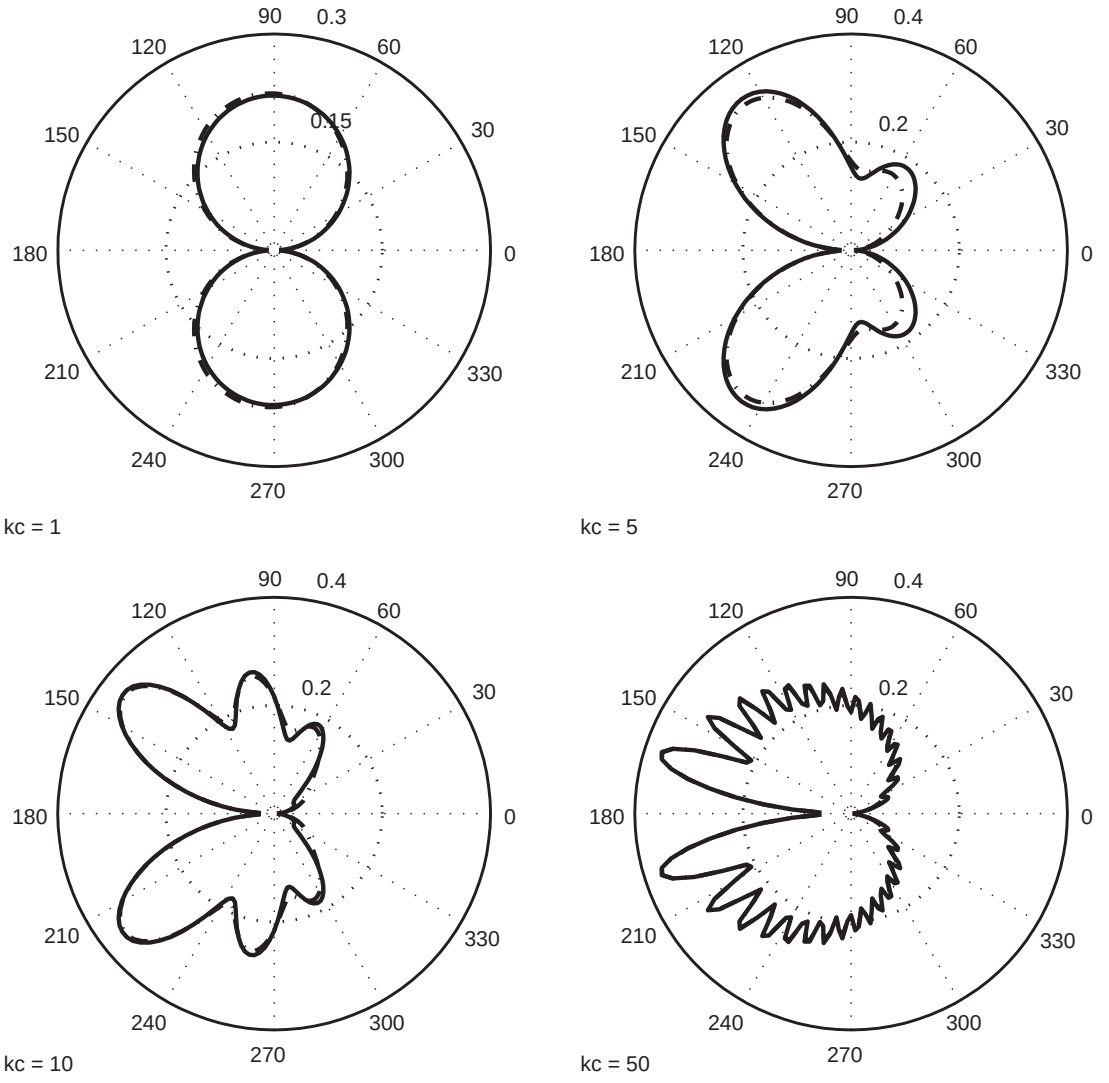

Fig. 6. Directivity patterns at high frequencies for comparison with [11]. $M = 0.05$, $\bar{K}_2 = 0$. —, full solution; -.-, main term only.

function tailored to a finite-chord flat plate, for sources close to the trailing edge. Both formulations are equivalent in the limit of very low Mach number flows. The advantage of the present approach is that it can be used at higher velocities.

Oblique gusts, with non-zero $\bar{K}_2$, depart progressively from the above behavior as $|\bar{K}_2|$ increases. Apparent singularities suggested by the possible values $B - C = 0$ and $D = 0$ in Eqs. (13) and (14) generate more focused radiation lobes, even in the mid-span plane, as shown in Fig. 7. It can be guessed that the higher efficiency of the radiation integral at the lobes is balanced by the smaller amount of energy of wall pressure fluctuations spread over the larger spanwise wavenumbers.

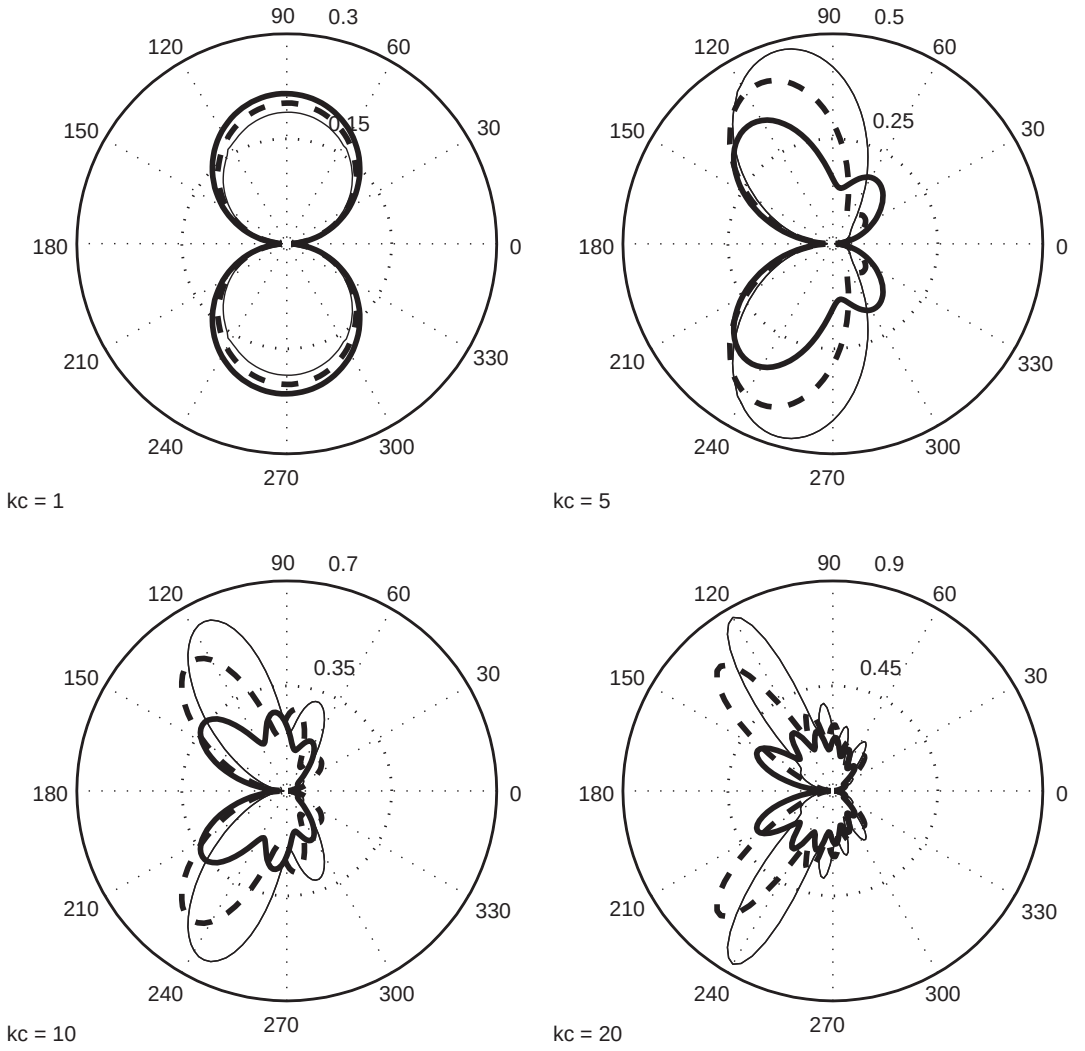

Fig. 7. Directivity patterns in the mid-span plane for various relative spanwise wavenumbers. $M = 0.05$, $\bar{K}_2/(\beta\bar{\mu}) = 0.05$. (——), 0.7 (- - -), 0.85 (——).

An analysis in terms of directivity patterns can also be made for subcritical gusts. First, a result equivalent to Eq. (13) can be derived in the same way, using the properties of the complex error function Φ° instead of E^*

$$\int_{-2}^{0} f_1'(X)\mathrm{e}^{-\mathrm{i}CX}\,\mathrm{d}X = -\frac{\mathrm{e}^{2\mathrm{i}C}}{\mathrm{i}C}\left\{\mathrm{e}^{-2\mathrm{i}C}\sqrt{\frac{A_1'}{\bar{\mu}(x_1/S_0)-\mathrm{i}\bar{\kappa}'}}\,\Phi^\circ([2\mathrm{i}(\bar{\mu}\,(x_1/S_0)-\mathrm{i}\bar{\kappa}')]^{1/2}) - \Phi^\circ([2\mathrm{i}A_1']^{1/2}) + 1\right\}. \quad (15)$$

Note that the term $\mathrm{e}^{-2\mathrm{i}C}$ has already been dropped in Eq. (15).

Secondly, the radiation integral for P_2 is obtained using the same derivation techniques

$$\int_{-2}^{0} f_2'(X)\mathrm{e}^{-\mathrm{i}CX}\,\mathrm{d}X = \frac{\mathrm{e}^{-2\mathrm{i}B}}{B}H'\left\{A'(\mathrm{e}^{2\mathrm{i}B}[1-\mathrm{erf}(\sqrt{4\bar{\kappa}'})]-1)+\sqrt{2\bar{\kappa}'}\left(\bar{K}+\left(M-\frac{x_1}{S_0}\right)\bar{\mu}\right)\frac{\Phi^{\circ}(\sqrt{-2\mathrm{i}B})}{\sqrt{-\mathrm{i}B}}\right\} \quad (16)$$

with

$$H' = \frac{(1+\mathrm{i})(1-\Theta'^2)}{2\sqrt{\pi}(\alpha-1)\bar{K}\sqrt{A_1'}}.$$

Typical diagrams in the mid-span plane are again given in Fig. 8 with the same convention as in Fig. 6. Subcritical gusts appear to radiate preferentially in directions normal to the airfoil. Roughly speaking, the aforementioned main lobe angle observed in the supercritical regime has progressively increased upto 90° at cut-off ($\bar{\kappa}=0$). Then, with increasing $\bar{K}_2$, it can be shown that it keeps the same direction and drops, according to what is expected qualitatively for rapidly decaying solutions. Again, the attenuation effect of the leading-edge correction at the smallest reduced frequency may be partially an artifact of the approximation made in P_2. Its validity will be assessed later.

A first test on the behavior around the cut-off is made by plotting $|I(\bar{\omega}/U_c,\bar{K}_2)|$ as a function of $\bar{K}_2$ over the whole range of both supercritical and subcritical gusts in Figs. 9 and 10. The radiation integral is computed using either the trailing-edge main scattering P_1 only, or the full solution including leading edge back-scattering. It is found that the leading-edge correction generally has a noticeable effect on the radiation integral, except for subcritical gusts at higher wavenumbers. Its main effect, depending on the radiation angle, is around the cut-off, where it ensures a more reliable behavior. However, deep, narrow cuts occur exactly at the cut-off, which suggests errors with respect to the expected continuous transition in the exact solution. The lower the frequency is, the larger the errors are. The Mach number effect combines with the frequency effect on the results. The cut-off is less effective at higher Mach numbers. Furthermore, the combination of high frequency and high Mach number does not show significant difference between the full solution and the one using P_1 only.

The sharp cuts are attributed to the breakdown of the present two-step solution at cut-off, where the proposed approximations fail because the frequency parameter $\bar{\kappa}$ in the equivalent 2D Schwarzschild problem is exactly zero. In that sense, the two derived P_2 expressions are asymptotic solutions that need to be properly matched at cut-off. Similar derivations by Landahl [22] suggest that the third and subsequent terms in the iterative procedure can be neglected in most applications of Schwarzschild's technique, provided the frequency parameter is non-zero. However, a higher number of terms would be necessary around $\bar{\kappa}=0$, where the method converges with difficulty. These higher-order iterations cannot be derived analytically and their numerical investigation is out of the scope of the present study. Furthermore, deriving an arbitrary large number of terms would make the method cumbersome and inappropriate for the intended application. Physically a smooth transition between supercritical and subcritical gusts is expected. At high frequencies such a behavior is already observed with the P_1+P_2 solution except in a very narrow range around $\bar{\kappa}=0$, which suggests that the cuts are model artifacts. Therefore,

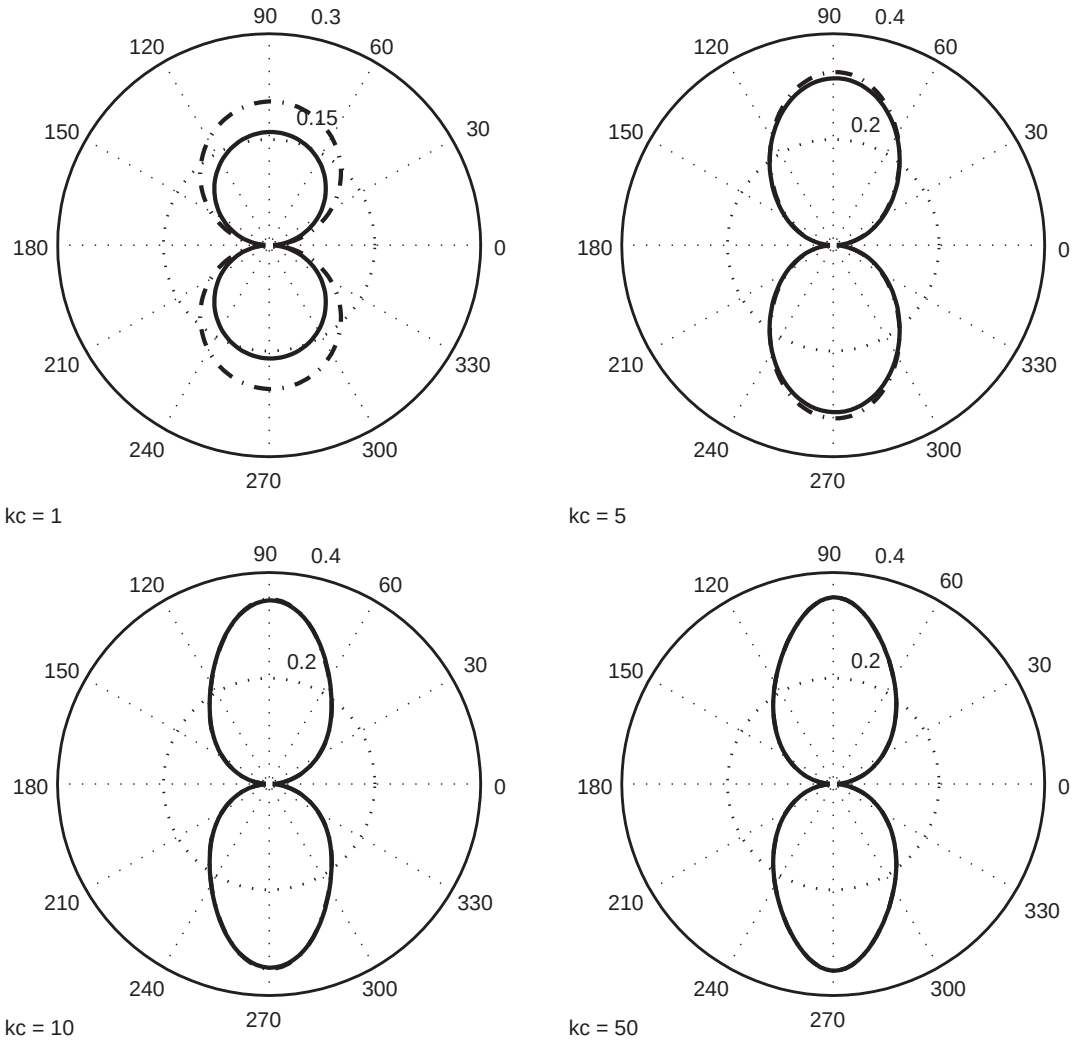

Fig. 8. Directivity patterns in the mid-span plane for subcritical gusts just below cut-off. $M = 0.05$, $\bar{K}_2/(\beta\bar{\mu}) = 1.05$. —, full solution; **-.-**, main term only.

a regularization technique has been applied to the $P_1 + P_2$ solution around the cuts to build a usable and more robust analytical model. This has been achieved by matching the values of the derivative $\partial I/\partial K_2$ from both sides of the cuts and then re-calculating I. The results of this regularization are superimposed on the non-corrected results in Fig. 11. Plots are made non-dimensional using the variable $\bar{K}_2/(\beta\bar{\mu})$. The calculations are made at different angles going from 20° to 160° in the mid-span plane and for two frequencies, with $c = 13\,\text{cm}$ and $M = 0.05$. At 200 Hz ($kc = 0.48$), I is almost independent of the angle θ from the downstream direction, whereas at 1000 Hz ($kc = 2.4$) it increases up to 140°. The behavior of subcritical solutions at higher values of $\bar{K}_2/(\beta\bar{\mu})$ is invariant. All profiles show a range of low spanwise wavenumbers in which the radiation integral is nearly constant, mainly corresponding to the supercritical range,

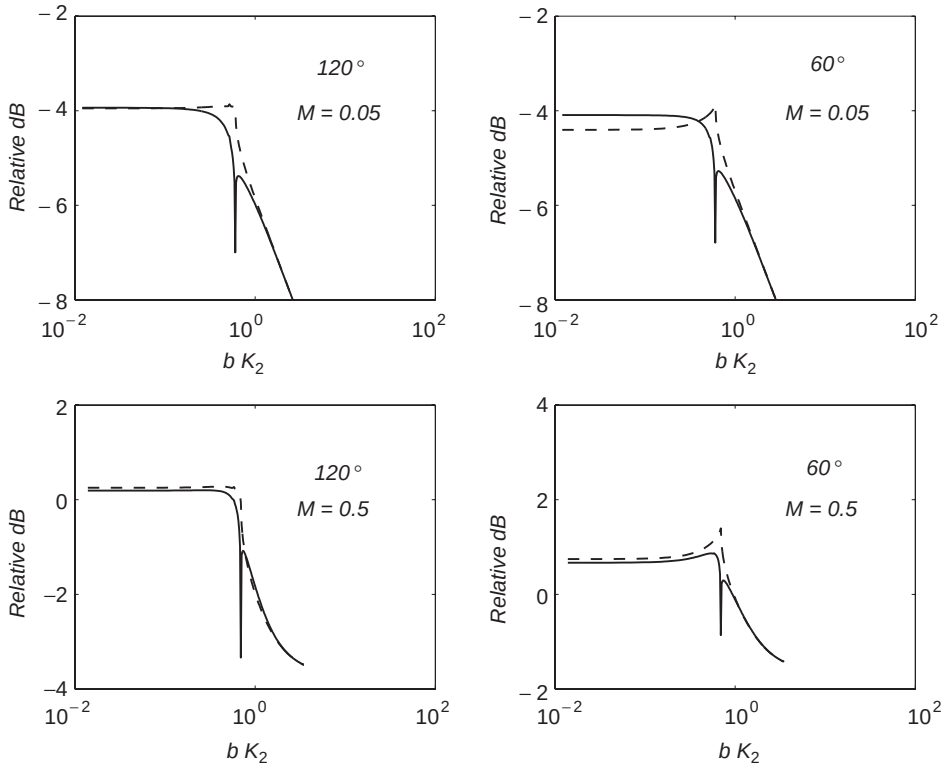

Fig. 9. Radiation integral profiles at 500 Hz for two radiation angles in the mid-span plane, with transition from supercritical to subcritical gusts. - - -, main term only; —, full solution.

and an asymptotic regular decrease for large wavenumbers, featuring the subcritical range. This decrease is steeper at higher frequencies. As a consequence of the results, the integral over $\bar{K}_2$ that is used to predict the far-field noise (see the next section) must include at least the beginning of the subcritical range. Furthermore, some amplification is observed as frequency increases for oblique supercritical gusts slightly below cut-off and angles below 120°. This amplification corresponds to the main lobe observed on the last plots in Fig. 7.

Moreover, the results of Fig. 11 help to assess the approximation made in P_2, by pointing out the limits of the range of $\bar{K}_2/(\beta\bar{\mu})$ in which the initially computed solution departs from the regularized one. On the basis of a chord length of 13 cm and the plots at 200 Hz, the solution is expected to be accurate enough for $\bar{\kappa} > 0.125$. This condition is equivalent to $kc/\beta^2 > 0.25$ in the case of the 2D problem, say a frequency larger than 100 Hz at reasonably low Mach numbers. This makes the first plots of Figs. 5 and 8 at the limit of validity. The latter limit is not a serious drawback for practical applications, as it is overcome by the regularization procedure. Moreover, 100 Hz is outside the range of significant loudness for human hearing.

The special problem of the leading-edge correction for the critical gust, for which $\bar{\kappa} = 0$, can be solved in the same way. The corresponding derivations are given in appendix Appendix A for completeness. They are not used here since the Schwarzschild's procedure does not converge at cut-off.

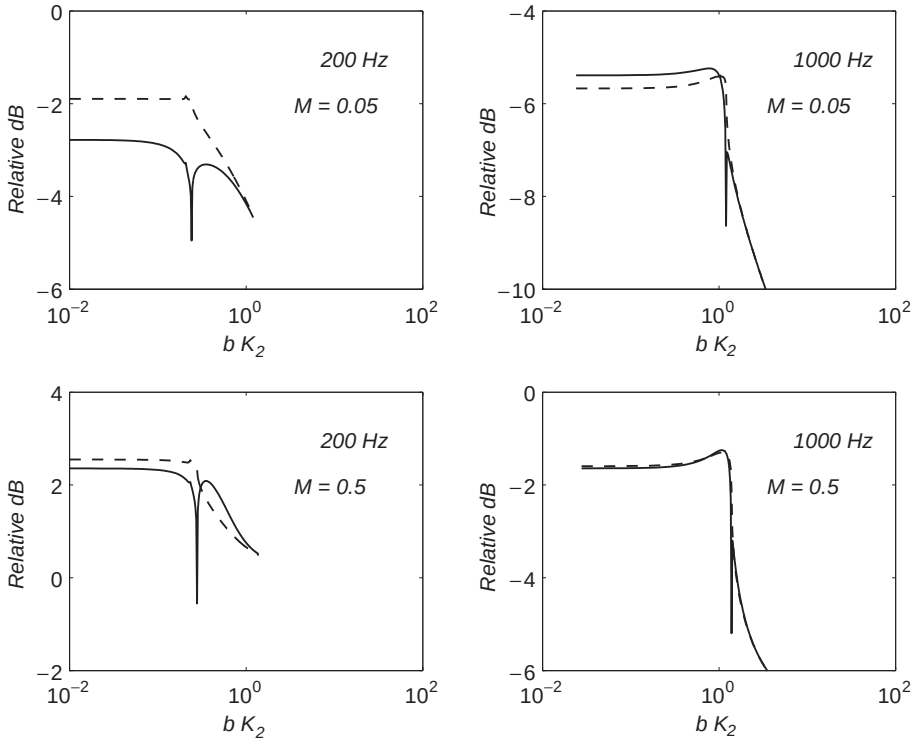

Fig. 10. Radiation integral profiles at 120° in the mid-span plane, with transition from supercritical to subcritical gusts. - - -, main term only; —, full solution.

4.2. Far-field acoustic power spectral density

The preceding radiation integral holds only for the unit gust with wavenumbers $(\bar{K}_1, \bar{K}_2)$ at reduced frequency ω. The power spectral density of the far-field sound at the same frequency results from an integration over all gusts with 2D wavenumbers contributing to this frequency. Amiet's arguments [21] may be reproduced to derive the result. Only the main steps are outlined here. The incident aerodynamic field is assumed frozen when convected past the airfoil trailing edge, which selects the streamwise aerodynamic wavenumber $K_1 = \omega/U_c$. The corresponding disturbance pressure distribution P over the airfoil surface is written as

$$P(x, y, \omega) = \frac{1}{U_c} \int_{-\infty}^{\infty} g\left(x, \frac{\omega}{U_c}, K_2\right) A_0\left(\frac{\omega}{U_c}, K_2\right) \mathrm{e}^{-\mathrm{i}K_2 y} \, \mathrm{d}K_2$$

with Amiet's function g (related to f of Section 3) formally denoting the transfer function between the incident pressure P_0 of amplitude A_0 and the disturbance pressure P, as calculated by the Schwarzschild's procedure. The incident wall pressure field induced by the turbulence developing on the airfoil is assumed a stationary random process. Consequently, P can be statistically analyzed. The corresponding cross-power spectral density between two points on the surface at

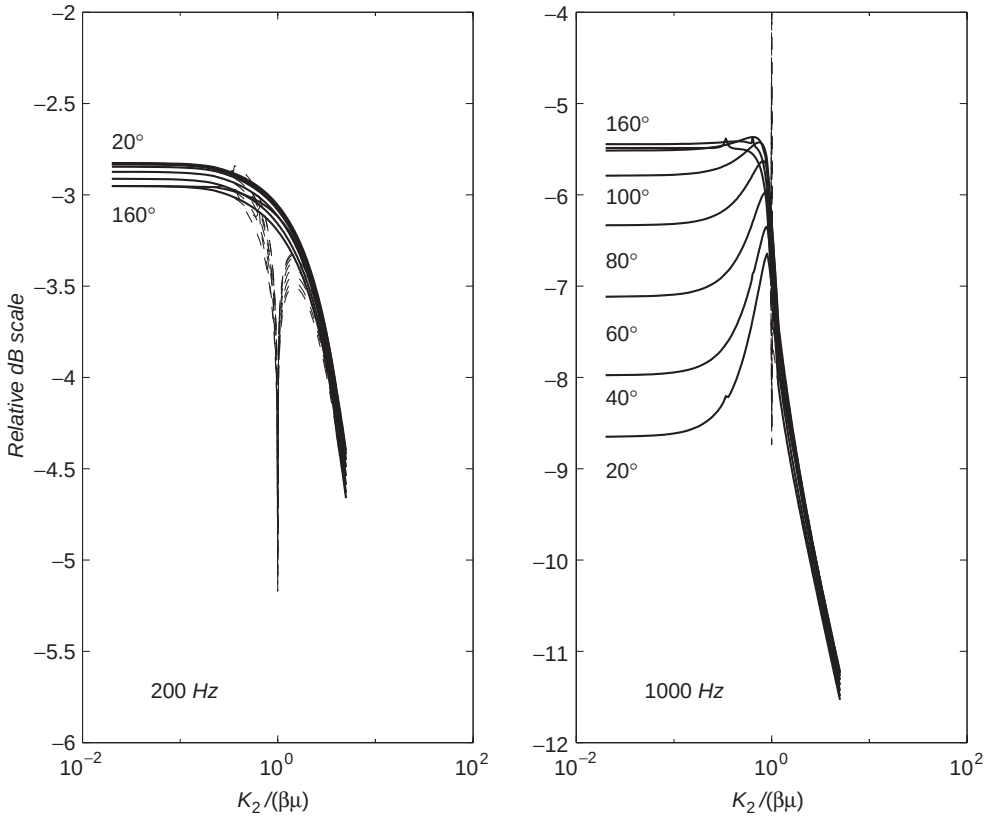

Fig. 11. Radiation integral profiles in non-dimensional variables. $M = 0.05$. - - -, regularization off; —, regularization on. Radiation angles from 20° to 160° by steps of 20°.

coordinates (x, y) and (x', y'), with $y - y' = \eta$, is then expressed as

$$S_{PP}(x, x', \eta, \omega) = \frac{1}{U_c} \int_{-\infty}^{\infty} g\left(x, \frac{\omega}{U_c}, K_2\right) g^*\left(x', \frac{\omega}{U_c}, K_2\right) \mathrm{e}^{-\mathrm{i}K_2\eta}\, \Pi_0\left(\frac{\omega}{U_c}, K_2\right) \mathrm{d}K_2,$$

where Π_0 denotes the wavenumber spectral density of the incident gust amplitudes A_0. The corresponding power spectral density (PSD) of the far-field sound is

$$S_{pp}(\mathbf{x}, \omega) = \left(\frac{\omega x_3 L b}{2\pi c_0 S_0^2}\right)^2 \frac{1}{b} \int_{-\infty}^{\infty} \Pi_0\left(\frac{\omega}{U_c}, K_2\right) \mathrm{sinc}^2\left\{\frac{L}{2b}\left(\bar{K}_2 - \bar{k}\,\frac{x_2}{S_0}\right)\right\} \times \left| I\left(\frac{\bar{\omega}}{U_c}, \bar{K}_2\right)\right|^2 \mathrm{d}\bar{K}_2. \tag{17}$$

The exact calculation using Eq. (17) can be involved within the scope of a fan design cycle. A major simplification is often made for a fast estimate by assuming that the aspect ratio L/b is large enough. This approximation is more acceptable if the characteristic scales of the aerodynamic

field close to the trailing edge are small enough when compared to the chord length. It is written as

$$\mathrm{sinc}^2\left\{\frac{L}{2b}\left(\bar{K}_2-\bar{k}\,\frac{x_2}{S_0}\right)\right\}\simeq\frac{2\pi b}{L}\,\delta\left(\bar{K}_2-\bar{k}\,\frac{x_2}{S_0}\right),$$

which selects a privileged oblique gust for each angle of radiation off the mid-span plane, and leads to

$$S_{pp}(\mathbf{x},\omega)=\left(\frac{\omega x_3 b}{2\pi c_0 S_0^2}\right)^2 2\pi L\left|I\left(\frac{\bar{\omega}}{U_c},\ \bar{k}\,\frac{x_2}{S_0}\right)\right|^2 \Pi_0\left(\frac{\omega}{U_c},\ k\frac{x_2}{S_0}\right). \tag{18}$$

This simplified result may become questionable, however, when applied to a fan. In that case, a blade must be discretized into several segments with limited spanwise extent because different relative velocities and flow conditions are encountered at different radial locations. As a consequence, the equivalent ratio L/b of each segment can be hardly considered as large. This will be investigated in the validation of Part 2.

Any noise calculation using Eqs. (17) or (18) requires as input the value of Π_0, that represents the energy of the incident wall pressure fluctuations at frequency ω for a given spanwise wavenumber. However, the derivation has been made assuming a frozen aerodynamic field. The real aerodynamic field is not frozen, and can only be reduced for statistical purposes to the full cross-spectral density function of the incident wall pressure $\Pi(K_1,K_2,\omega)$. If Π is considered as a quantity that can be determined elsewhere, either from experiments or from computations, then the total amount of energy at frequency ω is accounted for using the identity

$$\Pi_0\left(\frac{\omega}{U_c},\ \mu\,\frac{x_2}{S_0}\right)=\int_{-\infty}^{\infty}\Pi\left(K_1,\ k\,\frac{x_2}{S_0},\ \omega\right)\mathrm{d}K_1.$$

In fact, Π represents so huge an amount of information that it can hardly be fully reproduced from experimental results. Only partial measurements have been reported for some very simple flows or some airfoil shapes that can differ considerably from the ones to be investigated. The necessary flow statistics, even though essential are most often not available. They can be provided by accurate computational fluid dynamics methods such as Direct Numerical Simulation or Large Eddy Simulation. However, these simulations are only available for limited canonical test cases and unsuited to practical Reynolds numbers. For short-term acoustic calculations, the so-called Corcos' model [27] is thus often used, even though it was originally proposed to fit measured data for a fully turbulent boundary layer over a flat plate with zero pressure gradient. The boundary layers over curved surfaces such as the suction side of an airfoil may not follow the same properties. Strictly speaking, the first step in this model is the assumption of a statistically homogeneous wall pressure field close enough to the trailing edge that allows separation of the variables in the following way:

$$\Pi(K_1,K_2,\omega)=\frac{\Phi_{pp}(\omega)}{4\pi^2}\int_{-\infty}^{\infty}B\left(\frac{\omega}{U_c}\,|\eta_2|\right)\mathrm{e}^{\mathrm{i}K_2\eta_2}\,\mathrm{d}\eta_2\int_{-\infty}^{\infty}A\left(\frac{\omega}{U_c}\,|\eta_1|\right)\mathrm{e}^{\mathrm{i}(K_1-\omega/U_c)\eta_1}\,\mathrm{d}\eta_1.$$

In this factorization, Φ_{pp} is the wall pressure spectrum corresponding to the incident aerodynamic fluctuations only. In experiments, it can be measured by flush-mounted sensors and must be nearly constant in the investigated trailing-edge area. A and B are two decreasing functions of the

separation distances η_1 and η_2, that characterize the streamwise and spanwise correlation lengths, respectively. In the original Corcos' model, they are exponential functions, indicating that the correlation decreases with both increasing separation and frequency. Corcos' hypothesis has been re-visited by Singer [28], who showed using LES that, irrespective of the 1D functions A and B, the factorization leads to erroneous values of the model oblique wavenumber statistics. Spanwise and chordwise separations cannot be considered as independent variables. Moreover, in the case of an airfoil, different statistical features can be observed, as reported in Ref. [19], depending on the loading conditions. For instance A and B may be functions that do not decrease monotonically with increasing frequency. As a result, the most general definition of A and B must be considered here. Furthermore, Corcos' hypothesis appears not to be necessary for the present acoustic formulation.

Indeed let us introduce

$$\Pi(K_1, K_2, \omega) = \frac{1}{4\pi^2} \iint \Omega_{pp}(\eta_1, \eta_2, \omega)\, \mathrm{e}^{\mathrm{i}(K_1\eta_1 + K_2\eta_2)}\, \mathrm{d}\eta_1\, \mathrm{d}\eta_2,$$

where Ω_{pp} is the cross-spectral density between signals at two points on the airfoil with separations η_1 and η_2 in the streamwise and spanwise directions. Then A and B are defined as [28]

$$A(\eta_1, \omega) = \frac{\Omega_{pp}(\eta_1, 0, \omega)}{\Phi_{pp}(\omega)}, \quad B(\eta_2, \omega) = \frac{\Omega_{pp}(0, \eta_2, \omega)}{\Phi_{pp}(\omega)}$$

and, without any assumption on the wall pressure statistics,

$$\int_{-\infty}^{\infty} \Pi(K_1, K_2, \omega)\, \mathrm{d}K_1 = \frac{\Phi_{pp}}{2\pi} \int_{-\infty}^{\infty} B(\eta_2, \omega)\, \mathrm{e}^{\mathrm{i}K_2\eta_2}\, \mathrm{d}\eta_2.$$

The chordwise statistics are found to have no effect on trailing-edge noise. This is not surprising on the basis of physical arguments, since the scattering process only involves a change in the vortical field at the very trailing edge. However, since the sources are distributed all over the trailing edge, the spanwise statistics are of major importance.

The more tractable parameter from experiments is the wall pressure field coherence between two points on the airfoil surface

$$\gamma^2(\eta_1, \eta_2, \omega) = \frac{|\Omega_{pp}(\eta_1, \eta_2, \omega)|^2}{\Phi_{pp}^2(\omega)}.$$

Therefore, the coherence can be identified as the squared chordwise and spanwise correlation functions, A and B, respectively, when the separation η_2 or η_1 is set to zero. In most previously published experiments [17,19], the measurements are made in the mid-span plane and the only relevant spanwise wavenumber according to Eq. (18) is $K_2 = 0$. Then the far-field noise is shown to be proportional to the spanwise correlation length defined as

$$l_y(\omega) = \frac{1}{2} \int_{-\infty}^{\infty} B(\eta_2, \omega), \quad \mathrm{d}\eta_2 = \int_0^{\infty} \sqrt{\gamma^2(\omega, \eta_2)}\, \mathrm{d}\eta_2.$$

Apart from the mid-span plane, $l_y(\omega)$ must be replaced by the corrected correlation length

$$l_y(K_2, \omega) = \int_0^{\infty} \sqrt{\gamma^2(\eta_2, \omega)}\, \cos(K_2\eta_2)\, \mathrm{d}\eta_2.$$

In the special case of Corcos' model, this leads to the classical result

$$B(\eta_2,\omega)=\mathrm{e}^{-\omega|\eta_2|/(b_cU_c)},\quad l_y(\omega)=\frac{b_cU_c}{\omega},\quad l_y(K_2,\omega)=\frac{\omega/(b_cU_c)}{K_2^2+\omega^2/(b_cU_c)^2},\tag{19}$$

b_c being a constant. In more general cases, the correlation lengths are to be calculated using an appropriate model for the coherence. Finally, broadband trailing-edge noise can be predicted using Eqs. (18) or (17) together with

$$\Pi_0\left(\frac{\omega}{U_c},\ k\,\frac{x_2}{S_0}\right)=\frac{1}{\pi}\,\Phi_{pp}(\omega)\,l_y\left(k\,\frac{x_2}{S_0},\ \omega\right).\tag{20}$$

The present result is a revised form Eq. (4) in Ref. [9].

5. Conclusion

The problem of broadband trailing-edge noise modelling, as stated by Amiet [9], has been revisited by adding a leading-edge back-scattering correction and a 3D extension to the original formulation. Equations have been proposed for an intended application to fan noise prediction, using the aerodynamic wall pressure statistics close to the blade trailing-edge as input data. The wall pressure field is split into 3D either supercritical or subcritical gusts, each with their individual radiation efficiency. The leading-edge back-scattering is shown to be significant not only for small reduced frequencies but also when subcritical gusts are included in noise calculations off the mid-span plane, and more specifically at low Mach numbers. It must be accounted for, depending on the audible frequency range of interest and depending on the required accuracy. For large wind-turbine blades, for instance, it may certainly be neglected. It is important, however, for blades with a small chord length, such as those of automotive fans, since in that case kc typically ranges from 0.1 to 10. Therefore, the interest of the present analysis is two-fold. Firstly, it proves the validity of Amiet's primary work limited to the main trailing-edge scattering only, for application to large blades. Secondly, it provides a simple extension for other configurations of industrial interest. The proposed formulae are physically consistent in the sense that both the directivity and the frequency distribution are properly included. The application to a rotating fan blade segment in open air can be derived simply, as long as the rotational frequency remains smaller than the characteristic frequencies of trailing-edge noise, using the method reported by Paterson and Amiet [29] or Schlinker and Amiet [6]. The only restrictions are that the blade tip effects be ignored, on the one hand, and that a blade behave in the same way as an isolated airfoil, on the other hand. The latter point is justified by the fact that trailing-edge noise sources are not blade-to-blade correlated. It can be guessed that the analytical model applies better to unducted fans with a blade chord substantially smaller than the inter-blade spacing. In the case of ducted fans, an in-duct formulation is best suited, and an excellent analytical solution has been provided by Glegg [30].

The incident wall pressure statistics needed as input in the model may be the stumbling block for practical applications. It is missing in the RANS codes that are extensively used by manufacturers and that only provide statistical parameters of the fluctuating velocity field. The wall pressure data could be provided in the future by more sophisticated flow computations, such

as incompressible LES. However, fast-running alternative methods remain a real need for short-term purposes, especially in view of the great variety of flow regimes encountered in rotating blade technology. Experimental studies dedicated to the characterization of these regimes, such as flow separation at high loads, are still a point of interest. As a matter of fact, the present theory only addresses the question of the transfer function between the aerodynamic wall pressure and the far-field acoustic pressure, assumed independent of the flow conditions. Additional modelling of the relationship between the velocity statistics and the wall pressure statistics is a subject for future investigations.

Appendix A. 3D critical gusts ($\bar{\kappa} = 0$)

The critical solution is derived here for both the main contribution P_1 and the correction P_2. The main contribution is straightforward, for instance as a limit value of the exact supercritical solution as κ goes to zero, and leads to

$$P_1^0(X,0) = \mathrm{e}^{-\mathrm{i}\alpha\bar{K}X}[(1+\mathrm{i})E^*(-[\alpha\bar{K}+M\bar{\mu}]X) - 1].$$

Specific developments are to be made for the leading-edge correction since its approximations for subcritical and supercritical gusts fail at cut-off. The new expression for the correction potential is

$$\phi_2^0(X,0) = \frac{-b(1+\mathrm{i})\,\mathrm{e}^{\mathrm{i}M\bar{\mu}X}}{\pi^{3/2}\rho_0 U(\alpha-1)\bar{K}\sqrt{2}\sqrt{\alpha\bar{K}+M\bar{\mu}}}(1-\Theta^2)\int_0^\infty \frac{\mathrm{d}x}{\sqrt{x}\,\sqrt{2+(X+2)x}\,(1+x)}$$

with $\Theta^2 = (\alpha\bar{K}+M\bar{\mu})/(\bar{K}+M\bar{\mu})$.

This form of the remaining integral, which does not depend on frequency, has an analytical solution [24], leading to

$$\phi_2^0(X,0) = \left(\frac{-b}{\rho_0 U}\right)\frac{(1+\mathrm{i})(1-\Theta^2)}{\pi^{3/2}(\alpha-1)\bar{K}\sqrt{\alpha\bar{K}+M\bar{\mu}}}\,\mathrm{e}^{\mathrm{i}M\bar{\mu}X}\,\frac{\arcsin(\sqrt{-X/2})}{\sqrt{-X/2}}.$$

Then the correction pressure is deduced from

$$\frac{P_2^0(X,0)}{F} = \left[\mathrm{i}(\bar{K}+M\bar{\mu}) - \frac{1}{2X}\right]\mathrm{e}^{\mathrm{i}M\bar{\mu}X}\,\frac{\arcsin(\sqrt{-X/2})}{\sqrt{-X/2}} + \frac{\mathrm{e}^{\mathrm{i}M\bar{\mu}X}}{2X}\sqrt{\frac{2}{X+2}}$$

with

$$F = \frac{(1+\mathrm{i})(1-\Theta^2)}{\pi^{3/2}(\alpha-1)\bar{K}\sqrt{\alpha\bar{K}+M\bar{\mu}}}.$$

The main trailing-edge contribution to the radiation integral is simply deduced from the supercritical solution (integral of f_1 in Section 4.1) by setting $\bar{\kappa} = 0$. After standard manipulations, the correction can be written as

$$\frac{1}{F}\int_{-2}^{0} f_2^0(X)\,\mathrm{e}^{-\mathrm{i}CX}\,\mathrm{d}X = \Psi\left(1 - \frac{\pi}{2}\,\mathrm{e}^{-2\mathrm{i}A^\circ}\right) + \frac{1}{2}[1-\Psi]\int_{-2}^{0}\mathrm{e}^{\mathrm{i}A^\circ X}\,G(X)\,\mathrm{d}X$$

with

$$G(X) = \frac{1}{X}\left\{\sqrt{\frac{2}{X+2}} - \frac{\arcsin\left(\sqrt{-X/2}\right)}{\sqrt{-X/2}}\right\}$$

$$A^\circ = \alpha\bar{K} + M\bar{\mu} - C, \quad \Psi = \frac{\bar{K} + M\bar{\mu}}{A^\circ}.$$

A very good approximation of G for further analytical derivations is

$$G(X) \simeq -\frac{1}{\sqrt{2\,(X+2)}} + \frac{\pi}{4}\left\{1 - \left(1 - \frac{4}{3\pi}\right)\left(\frac{X+2}{2}\right)^{1/4}\right\}$$

which yields

$$\frac{1}{F}\int_{-2}^{0} f_2^0(X)\,\mathrm{e}^{-\mathrm{i}CX}\,\mathrm{d}X = \Psi\left[1 - \frac{\pi}{2}\mathrm{e}^{-2\mathrm{i}A^\circ}\right] + \frac{1}{2}\,(1-\Psi)\left[\frac{1-\mathrm{e}^{-2\mathrm{i}A^\circ}}{\mathrm{i}A^\circ}\,\frac{\pi}{4}\right.$$
$$\left. -\sqrt{\frac{\pi}{A^\circ}}\mathrm{e}^{-2\mathrm{i}A^\circ}\,E(2A^\circ) - 2\left(\frac{\pi}{4} - \frac{1}{3}\right)\mathrm{e}^{-2\mathrm{i}A^\circ}(\Sigma)\right] \tag{21}$$

with $A^\circ = (\alpha\bar{K} + M\bar{\mu}) - C$ and

$$(\Sigma) = (-2\mathrm{i}A^\circ)^{-5/4}\gamma(5/4, -2\mathrm{i}A^\circ) = \frac{4}{5}\,{}_1F_1\left(\frac{4}{5}, 1+\frac{4}{5}, 2\mathrm{i}\,A^\circ\right)$$

γ being the incomplete gamma function and ${}_1F_1$ the confluent hypergeometric function [26].

References

[1] S.E. Wright, The acoustic spectrum of axial flow machines, *Journal of Sound and Vibration* 45 (2) (1976) 165–223.

[2] S.A.L. Glegg, S.M. Baxter, A.G. Glendinning, The prediction of broadband noise from wind turbines, *Journal of Sound and Vibration* 118 (2) (1987) 217–239.

[3] H.H. Hubbard, K.P. Shepherd, Aeroacoustics of large wind turbines, *Journal of the Acoustical Society of America* 89 (6) (1991) 2495–2507.

[4] R. Parchen, W. Hoffmans, A. Gordner, K.A. Braun, N.J.C.M. van der Borg, A.G.M. Dassen, Reduction of airfoil self-noise at low Mach number with a serrated trailing edge, in: *Sixth International Congress on Sound and Vibration*, Copenhagen, Denmark, 1999, pp. 3433–3440.

[5] T. Fukano, Y. Kodama, Y. Senoo, Noise generated by low pressure axial flow fans—1: modelling of the turbulent noise, *Journal of Sound and Vibration* 50 (1) (1977) 63–74.

[6] R.H. Schlinker, R.K. Amiet, Helicopter trailing edge noise, NASA CR-3470, 1981.

[7] T.F. Brooks, M.A. Marcolini, D.S. Pope, Airfoil self-noise and prediction, NASA RP-1218, 1989.

[8] J.E. Ffowcs Williams, L.H. Hall, Aerodynamic sound generation by turbulent flow in the vicinity of a scattering half-plane, *Journal of Fluid Mechanics* 40 (1970) 657–670.

[9] R.K. Amiet, Noise due to turbulent flow past a trailing edge, *Journal of Sound and Vibration* 47 (3) (1976) 387–393.

[10] M.S. Howe, A review of the theory of trailing-edge noise, *Journal of Sound and Vibration* 61 (3) (1978) 437–465.

[11] M.S. Howe, Edge-source acoustic Green's function for an airfoil of arbitrary chord with application to trailing-edge noise, *The Quarterly Journal of Mechanics and Applied Mathematics* 54 (1) (2001) 139–155.

[12] E. Manoha, B. Troff, P. Sagaut, Trailing edge noise prediction using large eddy simulation and acoustic analogy, *AIAA Journal* 38 (4) (2000) 575–583.

[13] B.A. Singer, K.S. Brentner, D.P. Lockard, G. Lilley, Simulation of acoustic scattering from a trailing edge, AIAA paper 99-0231, 1999.
[14] J. Casper, F. Farassat, A new time domain formulation for broadband noise predictions, *International Journal of Aeroacoustics* 1 (3) (2002) 207–240.
[15] A. Oberai, F. Roknaldin, T.J.R. Hughes, Computation of trailing edge noise due to turbulent flow over an airfoil, *AIAA Journal* 40 (11) (2002) 2206–2216.
[16] M. Wang, P. Moin, Computation of trailing-edge flow and noise using large-eddy simulation, *AIAA Journal* 38 (12) (2000) 2201–2209.
[17] T.F. Brooks, T.H. Hodgson, Trailing edge noise prediction from measured surface pressures, *Journal of Sound and Vibration* 78 (1) (1981) 69–117.
[18] R.K. Amiet, Effect of the incident surface pressure field on noise due to turbulent flow past a trailing edge, *Journal of Sound and Vibration* 57 (2) (1978) 305–306.
[19] M. Roger, S. Moreau, Trailing edge noise measurements and prediction for subsonic loaded fan blades, *AIAA Journal* 42 (3) (2004) 536–544.
[20] M. Roger, S. Moreau, M. Wang, Towards airfoil self noise prediction using wall-pressure statistics from LES and an analytical acoustic model, Center for Turbulence Research Annual Research Briefs, 2002.
[21] R.K. Amiet, Acoustic radiation from an airfoil in a turbulent flow, *Journal of Sound and Vibration* 41 (4) (1975) 407–420.
[22] M. Landahl, *Unsteady Transonic Flow*, Pergamon Press, New York, 1961.
[23] J.J. Adamczyk, The Passage of an infinite swept airfoil through an oblique gust, NASA CR-2395, 1974.
[24] I.S. Gradshteyn, I.M. Ryzhik, *Tables of Integrals, Series and Products*, Academic Press, New York, 1980.
[25] J.M.R. Graham, Similarity rules for thin aerofoils in non-stationary flows, *Journal of Fluid Mechanics* 43 (1970) 753–766.
[26] M. Abramowitz, I.A. Stegun, *Handbook of Mathematical Functions*, Dover Publications, New York, 1970.
[27] G.M. Corcos, The structure of turbulent pressure field in boundary-layer flows, *Journal of Fluid Mechanics* 18 (1964) 353–378.
[28] B.A. Singer, Turbulent wall-pressure fluctuations: new model for off-axis cross-spectral density, NASA CR-198297, 1996.
[29] R.W. Paterson, R.K. Amiet, Noise of a model helicopter rotor due to ingestion of turbulence, NASA CR-3213, 1979.
[30] S. Glegg, The response of a swept blade row to a three-dimensional gust, *Journal of Sound and Vibration* 227 (1) (1999) 29–64.